



# 1 Estimation of NO<sub>x</sub> and SO<sub>2</sub> Emissions from Sarnia, Ontario 2 using Mobile-MAX-DOAS and a NO<sub>x</sub>-Analyzer

3 Zoe Y. W. Davis<sup>1</sup>, Sabour Baray<sup>2</sup>, Chris A. McLinden<sup>3</sup>, Aida Khanbakhani<sup>2</sup>, William Fujs<sup>2</sup>,  
4 Csilla Csukat<sup>2</sup>, Jerzy Debosz<sup>4</sup>, Robert McLaren<sup>2</sup>.

5  
6 <sup>1</sup>Graduate Program in Earth and Space Science, York University, Toronto, M3J 1P3, Canada

7 <sup>2</sup>Centre for Atmospheric Chemistry, York University, Toronto, M3J 1P3, Canada

8 <sup>3</sup>Environment and Climate Change Canada, Toronto, M3H 5T4, Canada

9 <sup>4</sup>Air Quality Monitoring and Assessment Unit, Ontario Ministry of the Environment, Conservation and Parks,  
10 Etobicoke, M9P 3V6, Canada

11

12 *Correspondence to:* Zoe Y. W. Davis ([zoeywd@yorku.ca](mailto:zoeywd@yorku.ca)) or R. McLaren ([rmclaren@yorku.ca](mailto:rmclaren@yorku.ca))

13 **Abstract.** Sarnia, ON experiences pollutant emissions disproportionate to its relatively small size. The small size of  
14 the city limits traditional top-down emission estimate techniques (e.g., satellite) but a low-cost solution for emission  
15 monitoring is Mobile-MAX-DOAS. Measurements were made using this technique from 21/03/2017 to 23/03/2017  
16 along various driving routes to retrieve vertical column densities (VCDs) of NO<sub>2</sub> and SO<sub>2</sub> and to estimate emissions  
17 of NO<sub>x</sub> and SO<sub>2</sub> from the Sarnia region. A novel aspect of the current study was the installation of a NO<sub>x</sub> analyzer in  
18 the vehicle to allow real time measurement and characterization of near-surface NO<sub>x</sub>/NO<sub>2</sub> ratios across the urban  
19 plumes, allowing improved accuracy of NO<sub>x</sub> emission estimates. Confidence in the use of near-surface measured  
20 NO<sub>x</sub>/NO<sub>2</sub> ratios for estimation of NO<sub>x</sub> emissions was increased by relatively well-mixed boundary layer conditions.  
21 These conditions were indicated by similar temporal trends in NO<sub>2</sub> VCDs and mixing ratios when measurements  
22 were sufficiently distant from the sources. Leighton ratios within transported plumes indicated peroxy radicals were  
23 likely disturbing the NO-NO<sub>2</sub>-O<sub>3</sub> photostationary state through VOC oxidation. The average lower limit emission  
24 estimate of NO<sub>x</sub> from Sarnia was  $1.60 \pm 0.34$  tonnes hr<sup>-1</sup> using local 10 m elevation wind-speed measurements. Our  
25 estimates were larger than the downscaled annual 2017 NPRI reported industrial emissions of 0.9 tonnes NO<sub>x</sub> hr<sup>-1</sup>.  
26 Our lower limit estimate of SO<sub>2</sub> emissions from Sarnia was  $1.81 \pm 0.83$  tonnes SO<sub>2</sub> hr<sup>-1</sup>, equal within uncertainty to  
27 the 2017 NPRI downscaled value of 1.85 tonnes SO<sub>2</sub> hr<sup>-1</sup>. Satellite-derived NO<sub>2</sub> VCDs over Sarnia from the Ozone  
28 Monitoring Instrument (OMI) were lower than Mobile-MAX-DOAS VCDs, likely due to the large pixel size  
29 relative to the city's size. The results of this study support the utility of the Mobile-MAX-DOAS method for



30 estimating NO<sub>x</sub> and SO<sub>2</sub> emissions in relatively small, highly industrialized regions especially when supplemented  
31 with mobile NO<sub>x</sub> measurements.

## 32 **1 Introduction**

33 Differential Optical Absorption Spectroscopy (DOAS) is a remote sensing technique that quantifies tropospheric  
34 trace-gases using light spectra and the unique spectral absorption cross sections of trace-gases. DOAS has been used  
35 since its introduction by (Platt et al., 1979) to measure small molecular species including NO<sub>2</sub>, SO<sub>2</sub>, OH, BrO, NO<sub>3</sub>,  
36 NH<sub>3</sub>, ClO and others. One advantage of the technique is the potential for simultaneous quantification of multiple  
37 trace-gases (e.g., SO<sub>2</sub> and NO<sub>2</sub>) (Platt et al., 2008). The Multi-Axis DOAS (MAX-DOAS) method allows sensitive  
38 quantification of tropospheric pollutants by measuring scattered sunlight spectra at multiple viewing directions  
39 and/or elevation angles. Spectra measured at elevation angles close to horizon-pointing have high sensitivity to  
40 ground-level gases since the light paths are longer near the surface (Honninger et al., 2004). Ground-based MAX-  
41 DOAS measurements quantify total boundary layer pollution loading by determining tropospheric vertical column  
42 densities (VCDs) of trace-gases. These measurements are, therefore, well suited to measurement of total emissions  
43 into an air mass. VCDs are independent of boundary layer height, unlike mixing ratios, and are spatially averaged  
44 (horizontally and vertically) on the order of a few kilometres along the light path. Ground-based MAX-DOAS can  
45 also retrieve vertical profiles of aerosol extinction and trace-gases by combining MAX-DOAS data with radiative  
46 transfer modelling (Friess et al., 2006; Heckel et al., 2005; Honninger et al., 2004; Honninger and Platt, 2002; Irie et  
47 al., 2008; Wagner et al., 2004, 2011).

48 The recently developed Mobile-MAX-DOAS technique allows measurement of trace-gas emissions from a region of  
49 interest by driving the instrument around the region. The method can estimate emissions on a nearly hourly basis in  
50 a region with a spatial resolution of ~1 km. Mobile MAX-DOAS has been used to estimate NO<sub>x</sub> emissions from a  
51 shipping and industrial areas (Rivera et al., 2010), power-plants (Wu et al., 2017) and cities (Ibrahim et al., 2010;  
52 Shaiganfar et al., 2011, 2017), validate satellite and air quality modelled VCDs (Dragomir et al., 2015; Shaiganfar et  
53 al., 2015), estimate surface NO<sub>2</sub> mixing ratios from NO<sub>2</sub> VCDs (Shaiganfar et al., 2011), and determine the  
54 horizontal variability of trace-gas VCDs within satellite pixels (Wagner et al., 2010). Mobile-MAX-DOAS is a “top-  
55 down” approach for quantifying real-world emissions that can be used to validate “bottom-up” emission inventories  
56 (Shaiganfar et al., 2011).



57 Sarnia, Ontario, a small Canadian city, experiences pollutant emissions due to a large number of industrial chemical  
58 and oil processing facilities, vehicular exhaust from the Canada-U.S.A. international border crossing, emissions  
59 from large ships travelling through the St Clair River, vehicular traffic, residential heating and other anthropogenic  
60 emissions from the city populace, and transnational air pollution from Ohio, Illinois and Michigan (Oiamo et al.,  
61 2011). These sources contribute to increased levels of air pollutants such as  $\text{NO}_x$ , VOC's and  $\text{SO}_2$ , which are  
62 precursors of  $\text{PM}_{2.5}$  and  $\text{O}_3$  (Ministry of the Environment and Climate Change, 2015). Traditional “top-down”  
63 methods for quantifying pollutant emissions from small cities (e.g., satellite monitoring, aircraft studies) are limited  
64 by the small footprint. Additionally, in-situ air quality monitoring stations are limited by the bias towards near-  
65 surface emissions and under-sampling of elevated emissions (Tokarek et al., 2018).

66 The Mobile-MAX-DOAS method has advantages over satellite, aircraft and in-situ techniques. Major advantages  
67 over satellite techniques include 1) emissions can be estimated without the need for an a-priori vertical profile, 2)  
68 accuracy of estimates can increase rather than decrease for smaller source regions, and 3) emissions may be  
69 estimated many times per day. Satellite retrievals are useful for estimating “top-down” emissions on regional and  
70 global scales over long periods of time (Huang et al., 2014; Kim et al., 2014; Liu et al., 2016; McLinden et al.,  
71 2012). However, accuracy over small regions can be limited by insufficient pixel resolution due to horizontal  
72 averaging and retrieval reliance on modelled a-priori vertical profiles that may not resolve small regions (Heckel et  
73 al., 2011). Aircraft studies can quantify emissions from cities but are relatively expensive. Major advantages of the  
74 Mobile-MAX-DOAS method over aircraft techniques (Baray et al., 2018; Gordon et al., 2015) are that 1) MAX-  
75 DOAS VCDs are already vertically integrated, reducing the uncertainties due to interpolation of measurements at  
76 multiple flight altitudes and 2) MAX-DOAS studies are logistically easier to conduct. The Mobile-MAX-DOAS  
77 technique is a solution for quantifying pollutant emissions that complements the aforementioned techniques as well  
78 as in-situ monitoring, through the ability to observe localized surface based and elevated emissions.

79 An uncertainty associated with MAX-DOAS and satellite methods when estimating  $\text{NO}_x$  emissions from  $\text{NO}_2$   
80 measurements is the assumptions concerning the  $\text{NO}_x/\text{NO}_2$  relationship in the air mass, which can be variable both  
81 spatially and temporally. The  $\text{NO}_x/\text{NO}_2$  ratio is often assumed to be spatially constant, taken from literature based on  
82 the season, estimated using atmospheric modelling or occasionally taken from aircraft measurements when available  
83 (Rivera et al., 2010). In this study, we combined the Mobile-MAX-DOAS method with simultaneous mobile  $\text{NO}_x$



84 measurements ( $\text{NO}$ ,  $\text{NO}_2$ ,  $\text{NO}_x$ ) to increase knowledge of the  $\text{NO}_x/\text{NO}_2$  ratio in the air mass spatially and temporally  
85 in order to improve the accuracy of the  $\text{NO}_x$  emission estimates obtained from  $\text{NO}_2$  measurements. A stationary  
86 modular meteorological station was deployed in the airshed provided auxiliary meteorological information, typically  
87 a major source of uncertainty in Mobile-MAX-DOAS emission estimations. Hourly wind data measured at 10 m  
88 elevation (agl) were also available from local, permanent monitoring stations. Vertical wind profiles were modelled  
89 in high resolution (1 km x 1 km) using the version 3.9.1 Weather Research and Forecasting model (WRF) centred on  
90 Sarnia ( $42.9745^\circ$  N,  $82.4066^\circ$  W) in an attempt to improve upon emissions values calculated using near-surface  
91 wind-speed, since wind-speeds are expected to increase with altitude. However, inter-comparison of WRF modelled  
92 winds with measured near-surface winds during the study period indicated poor model performance (see  
93 Supplement S2.2 for detailed results). Emissions in this study were therefore calculated using the 10 m measured  
94 winds to provide lower limit estimates of the hourly emissions.

95 Our study objectives were to 1) examine the relationship between the  $\text{NO}_2$  near-ground mixing ratios and the  $\text{NO}_2$   
96 tropospheric VCDs, 2) determine  $\text{NO}_x$  and  $\text{SO}_2$  emissions from the city of Sarnia including industrial sources, 3)  
97 determine the impact of  $\text{NO}_x/\text{NO}_2$  variability on the accuracy of  $\text{NO}_x$  emission estimates, and 4) examine OMI  
98 satellite intrapixel  $\text{NO}_2$  homogeneity. This study aims to demonstrate the utility of this method for determining  
99 trace-gas emissions and monitoring pollutant transportation in Sarnia and similar urban/industrial areas.

## 100 **2 Experimental**

### 101 **2.1 Location and Instruments**

102 Measurements were conducted in and around the city of Sarnia ( $42.9745^\circ$  N,  $82.4066^\circ$  W), located in southwestern  
103 Ontario, Canada at the border with Port Huron, MI, U.S.A (Fig.1). The routes driven in the vehicle aimed to capture  
104 major  $\text{NO}_x$  and  $\text{SO}_2$  emission sources at different distances downwind, dependent on the prevailing wind conditions.  
105 The metro area has a population of ~72,000 (2016 census) and an area of ~165 km<sup>2</sup>. Sources of air pollution in this  
106 region include emissions from large ships, anthropogenic emissions from the cities of Sarnia and Port Huron,  
107 transport from the cities of Windsor and Detroit (60 km SW), the St Clair and Belle River power-plants (20 km  
108 SSW), oil refineries and chemical industry in Sarnia, and the cross-border traffic between Canada and the U.S.A.



109 along Highway 402. Emissions from ships along the St. Clair River, normally a major source, were absent during  
110 the time of our study since the canal had not opened for the season.

111 A mini-MAX-DOAS instrument (Hoffmann Messtechnik GmbH) measured scattered sunlight spectra during three  
112 days: 21/03/2017 to 23/03/2017 (“Days 1 to 3”) while mounted on top of a car in a backwards pointing direction.  
113 The instrument has a sealed metal box containing entrance optics, UV fibre coupled spectrometer and electronics.  
114 Incident light is focused on a cylindrical quartz lens (focal length = 40 mm) into a quartz fibre optic that transmits  
115 light into the spectrometer (OceanOptics USB2000) with a field of view approximately  $0.6^\circ$ . The spectrometer has a  
116 spectral range of 290–433 nm, a  $50\mu\text{m}$  wide entrance slit yielding a spectral resolution was  $\sim 0.6$  nm. The  
117 spectrometer is cooled and stabilized by a Peltier cooler. Spectrometer data was transferred to a laptop computer via  
118 USB cable. Spectra were obtained with an integration time of  $\sim 1$  minute with the continuously repeating sequence  
119 of viewing elevation angles ( $30^\circ$ ,  $30^\circ$ ,  $30^\circ$ ,  $30^\circ$ ,  $40^\circ$ ,  $90^\circ$ ). The vehicle was driven at a low but safe target speed of 50  
120  $\text{km hr}^{-1}$  when possible to provide a spatial resolution of  $\sim 1$  km, but speeds were occasionally up to  $80 \text{ km hr}^{-1}$  when  
121 necessary. Tropospheric VCDs were estimated from the  $30^\circ$  and  $40^\circ$  elevation angle spectra. The  $40^\circ$  spectra allow  
122 verification that aerosol levels were sufficiently low to determine VCDs without radiative transfer modelling since  
123 VCDs obtained from both angles should be equal within  $\pm 15\%$  under low to moderate aerosol loading conditions  
124 (Wagner et al., 2010). The cool temperatures in March aided in this as secondary organic aerosol loading tends to be  
125 low in this season due to an absence of biogenic emissions.

126 A Model 42 chemiluminescence NO-NO<sub>2</sub>-NO<sub>x</sub> Analyzer (Thermo Environmental Instruments Inc.) mounted in the  
127 vehicle measured NO, NO<sub>2</sub>, and NO<sub>x</sub> (NO+NO<sub>2</sub>) near-surface mixing ratios. A PTFE inlet tube (5m length and  
128 ID=1/4”) was mounted above the front vehicle window on the passenger side ( $\sim 1.5$  m above ground). The  
129 instrument alternately recorded average NO-NO<sub>2</sub>-NO<sub>x</sub> mixing ratios with a temporal resolution of 1 minute. Most of  
130 the routes were driven downwind of Sarnia on rural remote roads with little to no traffic such that NO<sub>x</sub> emissions  
131 from other vehicles were not a concern. When NO<sub>x</sub> from other vehicles was a potential concern, data was filtered  
132 out via careful note taking. The instrument indirectly measures NO<sub>2</sub> by subtracting the NO chemiluminescence  
133 signal obtained when air bypasses a heated Molybdenum (Mo) convertor from the successive total NO<sub>x</sub>  
134 chemiluminescence signal obtained when air passes over the Mo-convertor. The NO<sub>x</sub> analyzer can overestimate NO<sub>x</sub>  
135 and NO<sub>2</sub> due to the potential contribution of other non-NO<sub>x</sub> reactive nitrogen oxides (NO<sub>z</sub>) other than NO<sub>2</sub> that can



136 also be reduced to NO by the Mo converter ( $\text{HNO}_3$ , HONO, organic nitrates, etc.), leading to an overestimation  
137 (Dunlea et al., 2007). Since this overestimation is more important in low  $\text{NO}_x$  regions, only data with  $\text{NO}_x$  mixing  
138 ratios  $> 3$  ppb were used. Mixing ratios of  $< 3$  ppb  $\text{NO}_2$  were only measured outside of plume-impacted regions when  
139  $\text{NO}_2$  VCDs were also low. The potential error in  $\text{NO}_x/\text{NO}_2$  ratios is addressed further in section 3.2.  $\text{NO}_x$  mixing  
140 ratios can also have an error when successive NO and  $\text{NO}_x$  measurements occurred in areas with a significant  
141 temporal gradient in the  $\text{NO}_x$  emissions. Such gradients were seen due to passing vehicles or localized industrial  
142  $\text{NO}_x$  plumes. These data were removed based on records of passing vehicles and other local near-surface sources or  
143 whenever the  $\text{NO}_2$  mixing ratios were reported as negative. Few data points were removed because the routes driven  
144 were primarily rural roads with extremely low traffic density.

145 Aura satellite Ozone Monitoring Instrument (OMI) data were obtained for overpasses of the Sarnia, Ontario area for  
146 Days 1 and 3. Tropospheric  $\text{NO}_2$  VCDs are the NASA Standard Product Version 3.0 with AMFs recalculated using  
147 the Environment and Climate Change Canada regional air quality forecast model GEM-MACH. The OMI  
148 instrument makes UV-vis solar backscatter radiation measurements with a spatial resolution of  $13 \times 24 \text{ km}^2$  at nadir  
149 and up to  $28 \times 150 \text{ km}^2$  at swath edges (Ialongo et al., 2014). The  $\text{NO}_2$  detection limit of OMI is  $5 \times 10^{14} \text{ molec cm}^{-2}$   
150 (Ialongo et al., 2016). The OMI data used were screened for row anomalies that have affected OMI data since June  
151 2007 (Boersma et al., 2007).

## 152 **2.2 MAX-DOAS Determination of VCDs**

153 Trace-gas Differential Slant Column Densities (DSCDs) were obtained using the DOAS technique (Platt et al.,  
154 2008) with the spectral fitting range of 410-435 nm for  $\text{NO}_2$  at 293 K and 307.5-318 nm for  $\text{SO}_2$  at 293 K. All trace-  
155 gas cross-sections used were from (Bogumil et al., 2003). For both gases, spectral fits also included a Fraunhofer  
156 Reference Spectrum (FRS), Ring Spectrum created from the FRS,  $\text{O}_3$  cross-sections at 223 K and 297 K, and a  
157 third-order polynomial. The  $\text{NO}_2$  cross-section was included in the  $\text{SO}_2$  fits.  $\text{NO}_2$  DSCDs from Day 1 were fit  
158 against a single, same-day FRS obtained in a low-pollutant region near solar-noon time. These DSCDs were  
159 corrected for  $\text{SCD}(\text{FRS})$  and  $\text{SCD}(\text{Solar Zenith Angle (SZA)})$  contributions using the  $\text{DSCD}_{\text{offset}}$  method (Wagner et  
160 al., 2010). The  $\text{SCD}(\text{FRS})$  is the constant tropospheric trace-gas SCD component present in the FRS that causes an  
161 underestimation in the fitted DSCD. The  $\text{SCD}(\text{SZA})$  is the difference between the stratospheric trace-gas component  
162 in the FRS and the measured non-zenith spectra.  $\text{SCD}(\text{SZA})$  varies over time of day ( $t_i$ ), maximizing overestimation



163 in the DSCD early and late in the day. The sum of SCD(FRS) and SCD(SZA) is collectively known as the  
164  $DSCD_{offset}$ . The  $DSCD_{offset}(t_i)$  function was estimated by fitting a second order polynomial to multiple pairs of  
165 DSCDs of spectra (non-zenith and zenith from the same sequence), described in detail in (Wagner et al., 2010).  
166 The  $DSCD_{offset}$  polynomial is most accurate when successive spectra in each sequence observe similar mixing ratio  
167 fields, and measurements obtained many data-points over most of the daylight hours. However, routes on Days 2  
168 and 3 included driving in and out of both high and low  $NO_x$  regions within short time-periods and thus met neither  
169 of the requirements listed above for the  $DSCD_{offset}$  method. On these days, a second method was used where  $NO_2$   
170 DSCDs were fit against an FRS spectrum obtained close in time (<25 minutes) along each respective route in a low-  
171 pollutant region. The impacts of SCD(FRS) and SCD(SZA) on the retrieved DSCDs can be assumed to be negligible  
172 since each FRS was from a low-pollutant area and obtained close in time, respectively. This method was also used  
173 for the Day 1  $SO_2$  route since limited data were available but included background  $SO_2$  measurements close in time.  
174 For all routes trace-gas tropospheric VCDs were determined by assuming a single scattering event occurred for each  
175 photon such that the air-mass factor (AMF) depended only on the viewing elevation angle,  $\alpha$ ,  $AMF_{trop}(\alpha) \approx \frac{1}{\sin(\alpha)}$   
176 (Brinkma et al., 2008)(Wagner et al., 2010). This “geometric approximation” is most valid under low to moderate  
177 aerosol loading and has been shown to deviate from the typically more accurate radiative transfer modelling by up to  
178  $\pm 20\%$  under moderate aerosol loading (Shaiganfar et al., 2011). Day 1 VCDs were calculated following Eq. (1):

$$VCD_{trop} = \frac{DSCD_{meas}(\alpha, t_i) + DSCD_{offset}(t_i)}{\frac{1}{\sin(\alpha, t_i)}} \quad (1)$$

179 Days 2 and 3  $NO_x$  and Day 1  $SO_2$  VCDs were calculated following Eq. (2):

$$VCD_{trop} \approx \frac{DSCD_{meas}(\alpha, t_i)}{\frac{1}{\sin(\alpha, t_i)}} \quad (2)$$

180

### 181 2.3 Estimating Trace-gas Emissions from MAX-DOAS VCDs

182 Trace-gas emission estimates were calculated following a flux integral approximation Eq. (3):

$$E = \left[ \sum_i (VCD_{outflow,i} - VCD_{influx,i}) w_i \sin(\beta_i) ds \right] \frac{MW}{Av} \quad (3)$$



183 where  $VCD_{outflow,i}$  is the VCD measured at position  $i$  along the route  $s$  for distance  $ds$ ,  $VCD_{influx,i}$  is either the  
184 measured influx values or the estimated background VCD value,  $w_i$  is the wind-speed,  $\beta_i$  is the angle between the  
185 driving direction and the wind-direction,  $MW$  is the molecular weight of the target gas, and  $A_v$  is Avogadro's  
186 number. Transect routes were designed to observe both within and beyond emission impacted areas since routes  
187 encircling the emission sources were often not possible. Flux integrals were calculated using portions of the  
188 transects impacted only by the Sarnia urban/industrial plume in cases where plumes from other sources impacted the  
189 transect (i.e., Day 1; U.S.A. power-plant plumes). In these cases, the end-points of integration were chosen  
190 judiciously where  $NO_2$  VCDs and surface mixing ratios decreased to a minimum at the edge of the Sarnia emissions.  
191 This method assumes that the wind-field and trace-gas emission rates are constant during the time required to drive a  
192 route. The validity of this assumption improves with decreased time for driving route completion. The Sarnia region  
193 is ideal for this method since a small geographical area contains the majority of the emissions and is surrounded on  
194 three sides by rural regions with low anthropogenic emissions.

195 A potential source of uncertainty in Mobile-MAX-DOAS emission estimates is variation in the wind fields and/or  
196 source emission rates while driving (Ibrahim et al., 2010; Wu et al., 2017). Previous studies have estimated wind-  
197 fields from local meteorology stations (Ibrahim et al., 2010), meteorological models (Shabbir et al., 2016;  
198 Shaiganfar et al., 2011, 2017) or LIDAR measurements (Wu et al., 2017). In our study, wind field information was  
199 obtained from a Modular Weather Station (Nova Lynx 110-WS-25DL-N) we deployed near one of the driving  
200 routes at  $(42.8148^\circ, -82.2381^\circ)$  (Fig. 1) and from meteorological ground stations in the area (Fig. 1, Table S1, Fig.  
201 S1). The modular weather station measured wind-speed and direction, temperature, relative humidity, and  
202 barometric pressure at 2 m above the surface every 30 seconds. Wind data was available from the Sarnia-Lambton  
203 Environmental Association (SLEA) LaSalle Road  $(42.911330^\circ, -82.379900^\circ)$  and Moore Line  $(42.83954^\circ, -$   
204  $82.4208^\circ)$  meteorological stations that are located near the driving routes (Fig. 1). These stations were surrounded  
205 by fallow, flat farm-land for at least 4 km on each side and thus should reflect total boundary layer for plumes  
206 transported away from the city more than the urban stations (Fig. S1). The hourly wind-direction data from the  
207 modular and permanent stations exhibited similar values ( $\pm 10^\circ$ ) and trends on Day 1 (Fig. S2). Wind-directions for  
208 Days 2 and 3 were obtained by determining the angle of a vector drawn between the geographical locations of the  
209 maximum  $NO_2$  VCD enhancements and the industrial facilities expected to have emitted the plumes. These map-  
210 determined wind-directions were consistent ( $\pm 10^\circ$ ) with the data from the station(s) closest to the driving route.



211 Comparison of wind-speed data on Days 2 and 3 was not possible due to a technical issue with the modular weather  
212 station on these days.

213 The NO<sub>2</sub> VCD influx (background VCD) was estimated on Day 1 since measurement was impossible along the  
214 western border of Sarnia due to the road configuration and proximity of industrial emissions. A NO<sub>2</sub> VCD<sub>influx</sub> =  
215  $2 \times 10^{15}$  molec cm<sup>-2</sup> was estimated based on OMI satellite VCDs of  $\sim 1.5\text{--}3.5 \times 10^{15}$  molec cm<sup>-2</sup> from the area east of  
216 Sarnia that are expected to be similar to the NO<sub>2</sub> regime west of Sarnia. These pixels are expected to be unaffected  
217 by other sources. The influx would be expected to be impacted by vehicular and residential emissions from the small  
218 city of Port Huron, U.S.A., on the west side of the St Clair River (Fig. 1), which has limited industry but a moderate  
219 level of commercial vehicle activity due to border-crossings. A first order emission estimate of vehicular NO<sub>x</sub>  
220 emissions from Port Huron from daily reported traffic counts results in an upper limit of NO<sub>2</sub> influx VCD of  
221  $\sim 1 \times 10^{15}$  molec cm<sup>-2</sup> (see Supplement S4). True influx would vary along the length of the measurement transect,  
222 depending on what sources are upwind of the location. Halla et al. (2011) measured NO<sub>2</sub> tropospheric VCDs using  
223 MAX-DOAS in a similar region approximately 70 km south-east of Sarnia. The observed NO<sub>2</sub> VCDs in that study  
224 ranged from 0.01 to  $1.25 \times 10^{16}$  molec cm<sup>-2</sup> with a median value of  $2 \times 10^{15}$  molec cm<sup>-2</sup>, which is expected to be  
225 representative of background NO<sub>2</sub> columns in this region. The highest VCD in that study was attributed to the  
226 transport of industrial emissions from the Sarnia area and/or from Detroit, MI to the northwest and west of the site  
227 respectively (Halla et al., 2011). Based on the range of VCDs from literature, vehicular emission estimates and  
228 satellite measurements, a background VCD of  $2 \times 10^{15}$  molec cm<sup>-2</sup> is a reasonable estimate, and emissions sensitivity  
229 tests were conducted using influx VCDs of  $0.5\text{--}3 \times 10^{15}$  molec cm<sup>-2</sup> (Supplement S5). In contrast, the NO<sub>2</sub> VCD<sub>influx</sub>  
230 on Days 2 and 3 and SO<sub>2</sub> VCD<sub>influx</sub> on Day 1 were determined from the average VCDs measured in the low-  
231 pollution area of each transect.

### 232 **2.3.1 Determination of NO<sub>x</sub> emission estimates from NO<sub>2</sub> measurements**

233 NO<sub>x</sub> emissions were estimated using Equation 4 from the NO<sub>2</sub> flux integral and the average NO<sub>x</sub>/NO<sub>2</sub> ratio (NO<sub>x</sub> > 3  
234 ppb) measured by the NO<sub>x</sub>-analyzer along the route. The emission values were then corrected for expected NO<sub>x</sub> loss  
235 during transport using a NO<sub>x</sub> lifetime,  $\tau$ . NO<sub>x</sub> emission estimates were calculated as follows:



$$E_{NO_x} = E_{NO_2} * \frac{\overline{NO_x}}{NO_2} * e^{\left(\frac{y/w}{\tau}\right)} \quad (4)$$

236 where  $\tau$  is  $NO_x$  lifetime,  $w$  is wind-speed, and  $y$  is the distance between the  $NO_x$  source and the measurement  
237 location. For routes where individual  $NO_x/NO_2$  ratios deviated significantly from the route average, the  $NO_x$   
238 emission estimates were calculated by applying 1) the route-averaged  $NO_x/NO_2$  ratio and 2) individual  $NO_x/NO_2$   
239 ratios associated with each  $NO_2$  VCD point by point. Multiple factors determine  $NO_x$  lifetime in a plume. A  $NO_x$   
240 lifetime of 6 hours was used in this study based on considerations given in section 3.3. A sensitivity analysis was  
241 performed varying the lifetimes between 4-8 hours (Supplement S7). The conversion factors used to calculate  $NO_x$   
242 emissions for each route can be found in Table S8. The  $NO_x/NO_2$  ratios are more fully addressed in Section 3.2 and  
243 the  $NO_x$  lifetime is addressed in Section 3.3.

## 244 3 Results & Discussion

### 245 3.1 Relationship between $NO_2$ VCDs & $NO$ - $NO_2$ - $NO_x$ Analyzer Measurements

246 Figure 2 shows that enhancements in  $NO_2$  VCDs downwind of Sarnia were generally associated with  $NO_2$  surface  
247 mixing ratios enhancements during Days 1 and 2. This suggests that pollution from Sarnia was well-mixed within  
248 the boundary layer at the measurement locations, typically 14-23 km downwind of sources (Figs. 3 & 4). However,  
249 the ratio of  $NO_2$  VCD to  $NO_2$  mixing ratio was sometimes variable even during relatively short time periods when  
250 the boundary layer height was expected to be constant (Fig. 2a). This variability was probably due to the presence of  
251 multiple  $NO_x$  plumes that had originated from sources with different heights (i.e., stacks and surface sources) and  
252 emission rates.

253 In contrast to Days 1 and 2,  $NO_2$  VCD enhancements on Day 3 were not consistently associated with  $NO_2$  surface  
254 mixing ratio enhancements (Figs. 5 & 6). A large surface enhancement ( $NO_x=22$  ppb) was observed at the location  
255 of the VCD  $NO_2$  enhancements ( $\sim 2.5 \times 10^{16}$  molec  $cm^{-2}$ ) associated with the NOVA Chemicals industrial plume on  
256 route 2 (Figs. 5b & 6b) but not on route 1 (Fig. 5a & 6a). This discrepancy is likely due to the closer proximity of  
257 the driving route to the source compared with Day 1, combined with limited vertical mixing of the plume. The  
258 relatively long sampling time of the  $NO_x$  analyzer with a relatively fast driving speed on this route may also have led  
259 to an underestimation of the true  $NO_x$  values for this localized plume.



### 260 3.2 NO<sub>x</sub>/NO<sub>2</sub> Ratios

261 The NO<sub>x</sub>/NO<sub>2</sub> ratio is necessary to estimate NO<sub>x</sub> emissions from the source, given measurements of NO<sub>2</sub> VCD's  
262 (Eq. 4). Ratios of NO<sub>x</sub>/NO<sub>2</sub> (Table 2) measured along the routes on Days 1 and 3 were within 20% of the route-  
263 averaged value with a relative standard deviation of less than 12%. NO<sub>x</sub>/NO<sub>2</sub> ratios tended to increase at locations  
264 associated with transported plumes' centerlines, as expected due to an increase in NO emissions from the sources  
265 (see Fig. 7), and exhibited the greatest variability in air-masses affected by sources with different altitudes and  
266 emission rates. Day 1, route 1 exhibited variable NO<sub>x</sub>/NO<sub>2</sub> ratios due to emissions from the power-plants across the  
267 river in Michigan, residential and vehicular traffic, and industrial emissions (Figs. 3a & 7).

268 Potential errors may exist in the NO<sub>x</sub>/NO<sub>2</sub> ratio due to the presence of other NO<sub>z</sub> species in the air mass (e.g., HNO<sub>3</sub>,  
269 HONO, NO<sub>3</sub>, N<sub>2</sub>O<sub>5</sub>, organic nitrates, etc.) that are also converted to NO by the Mo-converter in addition to NO<sub>2</sub>  
270 (Dunlea et al., 2007). However, these errors are smaller than might be expected due to the presence of the error in  
271 both the numerator and the denominator of the NO<sub>x</sub>/NO<sub>2</sub> ratio, thus offsetting. For example, at an apparent  
272 NO<sub>x</sub>/NO<sub>2</sub> ratio of 1.40 (average in Table 2), a 10% and 30% error in the reported NO<sub>2</sub> due the presence of other NO<sub>z</sub>  
273 species gives rise to errors of only -2.6% and -6.6% in the measured NO<sub>x</sub>/NO<sub>2</sub> ratio respectively. Mathematically,  
274 the error in the NO<sub>x</sub>/NO<sub>2</sub> ratio gets larger as the percentage of NO in the total NO<sub>x</sub> increases. However, since most  
275 of the interfering NO<sub>z</sub> species are generated photochemically, or only at night (NO<sub>3</sub>, N<sub>2</sub>O<sub>5</sub>) increasing with reaction  
276 time and distance away from the source, the percentage of interfering species is smaller at higher values of total NO  
277 and NO<sub>x</sub>. Under significantly intense photochemical conditions in the MCMA-2003 field campaign in Mexico, the  
278 interference in the chemiluminescence monitors resulted in average NO<sub>2</sub> concentrations being 22% higher than  
279 those determined from spectroscopic measurements (Dunlea et al., 2007), which would give rise to an error in the  
280 NO<sub>x</sub>/NO<sub>2</sub> ratio of <5%. In the current study we estimate that the resultant negative bias in the measured NO<sub>x</sub>/NO<sub>2</sub>  
281 ratio does not exceed -5% for several reasons; i) we filter out low NO<sub>x</sub> data (<3ppb), ii) the emission integral is  
282 dominated by regions with high NO<sub>x</sub> that are spatially and temporally close to the sources and, iii) photochemistry  
283 was reduced during this spring campaign. The uncertainty that arises from potential errors in the NO<sub>x</sub>/NO<sub>2</sub> ratio is  
284 insignificant compared to other errors (see Supplemental Table S9). It is also worth noting that NO<sub>2</sub> measurements  
285 by the NO<sub>x</sub> analyzer are not directly used for the calculation of emissions; only the NO<sub>x</sub>/NO<sub>2</sub> ratio is used.



286 Previous Mobile-MAX-DOAS studies have relied on literature estimates of the  $\text{NO}_x/\text{NO}_2$  ratio (Shabbir et al., 2016;  
287 Shaiganfar et al., 2011) or estimated the ratio from a Leighton ratio calculated using local air quality station data  
288 (Ibrahim et al., 2010). In regions with many pollutant sources throughout (e.g., megacities), this ratio is expected to  
289 be horizontally and vertically inhomogeneous. The ratio can therefore be challenging to estimate and can increase  
290 the uncertainty of the  $\text{NO}_x$  emission estimate. Estimation of  $\text{NO}_x/\text{NO}_2$  ratios from near-surface monitoring stations  
291 can be problematic because the ratios are applied to a VCD but may reflect only local emissions (e.g., nearby  
292 vehicular exhaust) rather than the total boundary layer. In this study,  $\text{NO}_x$  data impacted by local emissions were  
293 removed. Also, the Sarnia emissions were expected to be well mixed to the surface since most of the transects were  
294 driven sufficiently far from the sources. Therefore, the near-surface  $\text{NO}_x/\text{NO}_2$  ratios should be representative for the  
295 altitude range of the dispersed  $\text{NO}_x$  plume(s). This hypothesis is supported by the similarity between the  $\text{NO}_2$   
296 surface and VCD temporal trends during the study, especially on Days 1 and 2 (Fig. 2).

### 297 3.3 $\text{NO}_x$ Lifetime

298 Various lifetimes of  $\text{NO}_x$ ,  $\tau$ , have been used in previous mobile MAX-DOAS studies for the calculation of  $\text{NO}_x$   
299 emissions from  $\text{NO}_2$  measurements: 6 hr in Germany (Ibrahim et al., 2010), 5 hr in Delhi (Shaiganfar, 2011), 5 hr in  
300 China (Wu et al., 2017) and 3 hr summer – 12 hr winter in Paris (Shaiganfar, 2017). In Beirle et al. (2011), the  
301 daytime lifetime of  $\text{NO}_x$  was quantified by analyzing the downwind patterns of  $\text{NO}_2$  measured by satellite  
302 instruments and shown to vary from ~4 hr in low to mid-latitude locations (e.g., Riyadh, Saudi Arabia) to ~8hr in  
303 northern locations in wintertime (e.g., Moscow, Russia). In a follow up study, Valin et al (2013) showed that one  
304 cannot assume that  $\tau$  is independent of wind speed and derived values of  $\tau$  from the satellite observations over  
305 Riyadh to be 5.5hr to 8 hr, corresponding to OH levels of  $5\text{-}8 \times 10^6$  molec  $\text{cm}^{-3}$  at high and low wind speeds.

306 Multiple factors determine  $\text{NO}_x$  lifetime in a plume, including season (e.g., insolation) (Liu et al., 2016), latitude,  
307 wind-driven dilution (Nunnermacker et al., 2000; Valin et al., 2013),  $\text{NO}_x$  emission rate and initial dilution  
308 (Nunnermacker et al., 2000), temperature, hydroxyl radical levels (OH) and precursors to OH including  $\text{O}_3$ ,  $\text{H}_2\text{O}$ ,  
309 and HONO. Very importantly, the daytime lifetime of  $\text{NO}_x$  is a nonlinear function of the  $\text{NO}_x$  concentration itself,  
310 having longer lifetimes at high and low concentrations with the shortest lifetimes at intermediate  $\text{NO}_x$  concentrations  
311 due the impact on OH levels in a non-linear feedback on its own lifetime (Valin et al., 2013). The  $\text{NO}_x$  lifetime is  
312 ultimately dependent on the OH levels since this dictates the loss rate of  $\text{NO}_2$  to its terminal sink ( $\text{NO}_2 + \text{OH} \rightarrow$



313 HNO<sub>3</sub>). However the presence of VOC's in the urban plume, which are catalytically oxidized forming O<sub>3</sub> in the  
314 presence of NO<sub>x</sub> and HO<sub>x</sub> (OH + HO<sub>2</sub>), can decrease the NO<sub>x</sub> lifetime due to their acceleration of the conversion of  
315 NO to NO<sub>2</sub> via peroxy radical reactions (RO<sub>2</sub>' + NO → NO<sub>2</sub> + RO'). Therefore, NO<sub>x</sub> lifetimes can vary both  
316 spatially and temporally (Liu et al., 2016), even within the same plume (Valin et al., 2013). Underestimation of the  
317 true NO<sub>x</sub> lifetime leads to overestimation of the NO<sub>x</sub> emissions, while an overestimate leads to underestimation of  
318 the emissions.

319 While photolysis of HONO is often the major source of OH in the morning boundary layer (Platt et al., 1980; Alicke  
320 et al., 2002), midday production of OH via photolysis of O<sub>3</sub> and subsequent reaction of O (<sup>1</sup>D) with water is  
321 frequently the dominant source of OH. Assuming O(<sup>1</sup>D) is in steady-state, it can be shown that when ozone  
322 photolysis is the main source of OH, the product of the mixing ratios of H<sub>2</sub>O and O<sub>3</sub> is proportional to the  
323 production rate of OH. In this study, the [H<sub>2</sub>O]\*[O<sub>3</sub>] product was calculated using surrounding station measurements  
324 (see Supplement S8.1). The [H<sub>2</sub>O]\*[O<sub>3</sub>] product indicates that mid-day OH production under the spring-conditions  
325 for Days 1 and 2 is only 10-25% of the expected OH production under warmer more humid summer-conditions,  
326 presuming that O<sub>3</sub> photolysis predominates. This might suggest OH levels were lower in our study than during  
327 summer, and hence NO<sub>x</sub> lifetimes longer, however we assume this with caution as the HONO production is not  
328 known nor are the loss rates of OH.

329 As mentioned, the presence of VOC's can decrease the lifetime of NO<sub>x</sub> under conditions where NO<sub>x</sub> is sufficiently  
330 high to dominate the peroxy radical reaction path. To test for the presence of VOC's in the plumes (in the absence  
331 of measurements), Leighton ratios,  $\phi$  (Leighton, 1961), were calculated at locations of maximum NO<sub>2</sub> VCD  
332 associated with Sarnia plumes. Leighton ratios were calculated following Eq. (5) (see Supplement S8.2 for details):

$$\phi = \frac{j_{NO_2}[NO_2]}{k_8[NO][O_3]} \quad (5)$$

333 where  $j_{NO_2}$  is the NO<sub>2</sub> photolysis rate,  $k_8$  is the temperature-dependent rate constant for the reaction between NO and  
334 O<sub>3</sub>. Leighton ratios equal to 1.0 indicate that NO, NO<sub>2</sub> and O<sub>3</sub> are in steady state with no significant interference  
335 from other species, while ratios of  $\phi$  greater than 1.0 imply the role of other peroxy radical species (e.g., RO<sub>2</sub>, HO<sub>2</sub>)  
336 in the conversion of NO to NO<sub>2</sub> (Pitts and Finlayson-Pitts, 2000). The NO<sub>2</sub>/NO ratios were obtained from the NO<sub>x</sub>  
337 analyzer measurements, O<sub>3</sub> mixing ratios were obtained from local monitoring stations during the same daytime



338 periods as the transects. Values of  $j_{\text{NO}_2}$  were estimated using SLEA Moore Line station solar irradiance data (Fig. 1;  
339 Table S1) and solar zenith angle following the method in Wiegand and Bofinger (2000).

340 Table 2 shows Leighton ratios calculated at the locations of maximum  $\text{NO}_2$  VCD enhancements. Calculated  
341 Leighton ratios were significantly greater than 1 (1.7-2.3) at peak  $\text{NO}_x$  locations on Day 1 (Table 2). We interpret  
342 this as an indication that significant levels of peroxy radicals were present in the plume, presumably from VOC  
343 oxidation by the OH radical. This is consistent with high VOC emissions from the petrochemical facilities in  
344 Sarnia, with emission rates  $>300$  tonnes  $\text{yr}^{-1}$  each for four of the top six industrial  $\text{NO}_x$  emitters in Sarnia  
345 (Environment and Climate Change Canada, 2018d). The Day 2 Leighton ratio of less than 1.0 in Table 2 suggests a  
346 relatively fresh plume (only 4 km downwind of a facility) that had not come to photo-stationary state.

347 Thus we have indications that OH production may be lower than summer time leading to longer  $\text{NO}_x$  lifetimes and  
348 we have indications that VOC oxidation in the plume may be significant leading to shorter  $\text{NO}_x$  lifetimes than air  
349 masses where the photo-stationary state in  $\text{NO}_x$  is valid. Without further information, we have opted to assume a  
350 central  $\text{NO}_x$  lifetime assume of  $\sim 6$  hr. Sensitivity calculations were conducted for  $\text{NO}_x$  emission estimates using a  
351 range of lifetimes of 4-8 hours (Supplement S7). Varying the lifetime from  $\pm 2$  hours changed the emission estimates  
352 by  $<15\%$  for all routes except for Day 1 route 1 due to low wind-speeds during that route (30% change).

353 For the calculation of  $\text{SO}_2$  emissions,  $\text{SO}_2$  was assumed to have a sufficiently long lifetime in the boundary layer so  
354 as to be conserved between the emission and measurement location. Note that cloud processing of  $\text{SO}_2$  was assumed  
355 to be negligible since  $\text{SO}_2$  measurements were completed on a mostly cloud-free day.

### 356 **3.4 Emission Estimates**

357

#### 358 **3.4.1 Emission Estimates of Sarnia**

359 The VCDs measured are shown in Fig. 3-6 while the  $\text{NO}_x$  emissions calculated using Eqs. (3) and (4) are shown in  
360 Table 4. The values of  $\text{VCD}_{\text{influx}}$  required for the calculations were typically determined from measurements of VCD  
361 in low pollution transect areas. However, the  $\text{VCD}_{\text{influx}}$  on Day 2 was not determined in this way since these DSCDs  
362 were close to zero within error (Figs. 2 & 4). The  $\text{VCD}_{\text{influx}}$  is expected to be low on Day 2 because the north wind-  
363 direction indicates that the air-masses originated from over Lake Huron. These low values were probably due to low



364 light levels during measurement, insufficiently long integration times (low signal to noise ratio) and NO<sub>2</sub>  
365 background VCD values below the instrument's limit of detection. A low value of VCD<sub>influx</sub> = 0.5(±0.5)×10<sup>15</sup> molec  
366 cm<sup>-2</sup> was therefore assumed.

367 The emissions were calculated in two ways i) using a route-average NO<sub>x</sub>/NO<sub>2</sub> ratio value for each route estimate and  
368 ii) using individual NO<sub>x</sub>/NO<sub>2</sub> ratios co-located with each VCD measurement. For Day 1 route, the route average  
369 NO<sub>x</sub>/NO<sub>2</sub> ratio was 1.53 ± 0.12 ppb ppb<sup>-1</sup> with the difference between the calculated emission rates using the two  
370 methods being only 3%. Day 1 transects 2-4 exhibited small variability in NO<sub>x</sub>/NO<sub>2</sub> (Table 4) and the variation in  
371 the NO<sub>x</sub>/NO<sub>2</sub> ratio impacted emission estimates by less than 5%.

372 However, the difference between emission estimates calculated using individual NO<sub>x</sub>/NO<sub>2</sub> ratios versus a route-  
373 averaged value can be non-trivial, as observed with the Day 2 route 1. Day 2 had consistent northerly wind  
374 conditions, and east-west transects were driven south of Sarnia to capture the urban plume and background regions  
375 to the east (Fig. 4). The resultant Sarnia NO<sub>x</sub> emission using the first method is consistent with the first three Day 1  
376 emission estimates but application of the second method (individual NO<sub>x</sub>/NO<sub>2</sub> ratios collocated with each VCD)  
377 increased the emission estimate by ~50% (Table 4 and Fig. 8). The NO<sub>x</sub>/NO<sub>2</sub> ratio was generally consistent with the  
378 averaged value of 1.3 (maximum NO<sub>x</sub>/NO<sub>2</sub> removed) but increased to 3 in the region of maximum NO<sub>2</sub> VCD  
379 enhancements 7 km south of the NOVA Chemicals facility (Table 3). The calculated Leighton ratio for this peak  
380 NO<sub>x</sub>/NO<sub>2</sub> ratio location is less than 1 (see 3.4.2 and Table 3). The Leighton ratio suggests the plume from the  
381 NOVA Chemical facility had significant NO that had not had sufficient time to come to a photostationary state. The  
382 emission estimate using individual NO<sub>x</sub>/NO<sub>2</sub> ratios is considered the more accurate value for this route compared to  
383 the emission value calculated using the route-averaged ratio.

384 The importance of measuring the local NO<sub>x</sub>/NO<sub>2</sub> ratio is also illustrated by observing variation of the ratio due to the  
385 impact of the Michigan power-plants' plume, apparent in the Day 1 route 1 East-West transect (Fig. 3a). The  
386 NO<sub>x</sub>/NO<sub>2</sub> ratio along this transect increased to ~1.7 (Fig. 7), higher than the maximum NO<sub>x</sub>/NO<sub>2</sub> ratio observed in  
387 the North-South transect downwind of Sarnia. A higher ratio is somewhat unexpected because the distance between  
388 the source and receptor measurement for the power plant source was greater than the source-receptor distance for the  
389 Sarnia sources. Thus, the power-plant plume would have been expected to be more aged, but the results suggest that  
390 the power-plants' plumes had a slower conversion of NO to NO<sub>2</sub> perhaps due to higher initial mixing ratios of NO<sub>x</sub>



391 (Nunnermacker et al., 2000). Very high NO mixing ratios in a power plant plume (i.e., > 40ppb) could completely  
392 titrate the ambient O<sub>3</sub> in the air entrained into the plume, an observation previously seen in power plant plumes  
393 (Brown et al., 2012).

394 The East-West transect appears to have captured approximately half of the power-plants' plume since the NO<sub>2</sub>  
395 VCDs and the NO<sub>2</sub> mixing ratios increase from background to a plateau at a maximum (Fig. 2a). A preliminary  
396 estimation of the NO<sub>x</sub> and SO<sub>2</sub> emissions from the power-plants can be determined by doubling the flux integral  
397 calculated from this East-West transect. To do this, we have used  $VCD_{influx} = 2-3 \times 10^{15}$  molec cm<sup>-2</sup> for NO<sub>x</sub> and zero  
398 for SO<sub>2</sub> since the background region SO<sub>2</sub> DSCDs were at or below detection limits. The NO<sub>x</sub> estimate used  
399 individual NO<sub>x</sub>/NO<sub>2</sub> ratios because the NO<sub>x</sub>/NO<sub>2</sub> ratio was significantly higher in the plume than outside the plume.  
400 This illustrates the importance of in-situ instruments of NO<sub>x</sub>/NO<sub>2</sub>, especially when close to the source where plume  
401 NO<sub>x</sub>/NO<sub>2</sub> ratios can be variable (Valin et al., 2013). Given the above assumptions, a tentative estimate of the total  
402 emissions from the power plants are 0.31-0.46 tonnes NO<sub>x</sub> hr<sup>-1</sup> and 0.77 tonnes SO<sub>2</sub> hr<sup>-1</sup>, respectively. The hourly  
403 emissions of the power-plants downscaled from reported 2015 annual values are 0.74 tonnes NO<sub>x</sub> hr<sup>-1</sup> and 2.56  
404 tonnes SO<sub>2</sub> hr<sup>-1</sup> (United States EPA, 2018). Our hourly estimates are only preliminary since only half of the plume  
405 (approximately) was captured by the measurement transect.

406 The NO<sub>x</sub> emission estimates from Sarnia from Day 1 are consistent within 25% and are consistent with the Day 2  
407 estimates within the calculated error of approximately ±45% (Fig. 8, Table 4). Some variability between the  
408 emission estimates is expected due to wind-data uncertainties, NO<sub>x</sub>/NO<sub>2</sub> vertical profile variability, errors introduced  
409 by using a constant  $VCD_{influx}$  and NO<sub>x</sub> lifetime, and temporal variations in emissions from the source.

410 Conversion of the hourly measured emissions to annual emissions would require knowledge and application of  
411 daily, weekly and seasonal emission profiles, which is beyond the scope of this work. The Mobile-MAX-DOAS  
412 emission estimates are reported in units of tonnes per hour since routes were completed within <40 minutes. Events  
413 such as flaring can significantly increase the instantaneous emission rate but are excluded from the annual emission  
414 inventory data. However, there was no reported flaring during the measurement period (MOECC 2017; personal  
415 communication). NO<sub>x</sub> emissions from petrochemical facilities, excluding flaring, typically have low variability  
416 during periods of continuous operation. According to Ryerson et al. (2003), variation in average hourly NO<sub>x</sub>  
417 emissions from a petrochemical facility reported by industry (CEMS data) was <10% from an average of the hourly



418 average emissions over 11 days in Houston, Texas. However, this trend may be different for the chemical industry.  
419 A first-order comparison to the 2017 National Pollution Release Inventory (NPRI) values (downscaled by assuming  
420 constant emissions) was made to determine whether our measured Sarnia emissions are reasonable. The NPRI value  
421 is the sum of the  $\text{NO}_x$  emissions from the top 9 industrial emitters of  $\text{NO}_x$  in Sarnia whose emissions would have  
422 been captured along the driving routes. The NPRI requires significant point source industry facilities to report their  
423 pollutant emissions, but the method of estimating emissions can vary by facility (Canada and Canada, 2015). The  
424 NPRI emission value does not include mobile and area sources from the Sarnia region. Thus, the NPRI emission  
425 inventory values for Sarnia would be expected to be smaller than our measured emissions because of this exclusion.  
426 The measured  $\text{NO}_x$  emissions are larger than the 2017 NPRI value but not statistically so (Fig. 8; Table 4). The  
427 exception is the Day 1 route 1\* value, which is statistically higher. The average of the four  $\text{NO}_x$  emission estimates  
428 from Sarnia is greater than the 2017 NPRI value. These results demonstrate that our measured emission rates are  
429 reasonable. Future Mobile-MAX-DOAS studies could focus on determining diurnal trends in emissions by driving  
430 multiple routes at as many times of the day as possible on multiple days, seasons and weekdays/weekends.  
431 Measurements of vertical wind profiles could reduce emission uncertainty to allow identification of temporal trends  
432 by comparing same-day measurements.

433 Apart from  $\text{NO}_x$ , we were also able to estimate  $\text{SO}_2$  emissions from the Sarnia urban/industrial region from the Day  
434 1 route 3 (Table 5). Our  $\text{SO}_2$  emission estimate using the 10 m wind-speed is consistent within error with the 2017  
435 NPRI value (Table 5). We expect our  $\text{SO}_2$  emission estimate to be closer to the NPRI values compared to the  $\text{NO}_x$   
436 estimates because  $\text{SO}_2$  emissions from area and mobile sources in Sarnia are expected to be small relative to  
437 industrial sources (Ministry of the Environment and Climate Change, 2016). Since ships were not operating in the  
438 St. Clair River at this time of year, shipping emissions of  $\text{SO}_2$  were absent. Thus  $\text{SO}_2$  plumes in this region are  
439 localized to the major industrial emissions sources. Therefore, the VCDs from the areas unaffected by the Sarnia  
440 plumes are representative of background values,  $\text{VCD}_{\text{influx}}$ . While the Mobile-MAX-DOAS was able to capture these  
441 plumes (Fig. 9), only 1 of 7 local monitoring stations (LaSalle Road, Fig. S1) observed elevated levels of  $\text{SO}_2$  during  
442 this period. The under-sampling by stations is due to the highly localized nature of the  $\text{SO}_2$  plumes that are from  
443 stacks where the plume is frequently elevated above the surface. These results illustrate the complementary nature of  
444 Mobile-MAX-DOAS and in-situ measurements and the importance of monitoring techniques that can capture  
445 localized plumes independent of the wind direction.



446 **3.4.2 Emission Estimates of NOVA Chemicals Industrial Facility**

447 NO<sub>x</sub> emissions were opportunistically measured from a single facility on Day 3 because the southerly wind-  
448 directions isolated this plume (Environment and Climate Change Canada, 2018b) from other industrial sources in  
449 Sarnia. The plume originated from Nova Chemicals, the 2<sup>nd</sup> highest emitter of NO<sub>x</sub> in the region in 2017. These  
450 conditions allowed us to test the mobile-MAX-DOAS method in isolating a single plume. The wind-direction on  
451 Day 3 indicated that the air-masses originated from rural areas south of Sarnia and the VCD<sub>influx</sub> was expected to be  
452 low,  $\sim 1 \times 10^{15}$  molec cm<sup>-2</sup>.

453 The emission estimates of NO<sub>x</sub> from the two routes on Day 3 from the NOVA Chemicals industrial site (Tables 4 &  
454 5) are consistent with each other within 10%. The consistency increases confidence in fitting the spectra in each  
455 transect against a local FRS and removing influx using the average “background” VCDs rather than using the  
456 “DSCD<sub>Offset</sub>” method in this case. The use of “background” VCDs is appropriate because vehicular traffic upwind of  
457 the measurement transect is minimal in the local area. Upwind emissions were unlikely to have contributed  
458 significantly to the total measured emissions. The emission estimates from NOVA Chemicals are larger than the  
459 2017 NPRI value (Tables 4 & 5). This comparison merely indicates that the Mobile-MAX-DOAS values are  
460 reasonable given that there was likely diurnal variability and the measurements were taken only during a single hour  
461 on a single day.

462 **3.5 Comparison of OMI Satellite and MAX-DOAS VCDs**

463 The satellite and MAX-DOAS NO<sub>2</sub> VCDs on Day 1 exhibit similar spatial trends in the simple sense that NO<sub>2</sub>  
464 VCDs increase towards the south from the background regions north of Sarnia (Fig. 10). This trend is probably due  
465 to a combination of emissions from U.S.A. power-plants, the Detroit area as well as Sarnia. The NO<sub>2</sub> VCD of the  
466 pixel containing the majority of the Sarnia industrial facilities is comparable to rural area VCDs to the north-west of  
467 Sarnia. Only 1/8<sup>th</sup> of the “Sarnia” pixel’s footprint region is likely to be impacted by Sarnia emissions, and the  
468 remainder observes mostly rural to semi-rural regions. The OMI Pixel from Day 3 (Fig. 11) containing Sarnia  
469 exhibits a minimal increase in NO<sub>2</sub> VCD ( $1-2 \times 10^{15}$  molec cm<sup>-2</sup>) compared to the surrounding background regions  
470 (Fig. 11). In contrast, the Mobile-MAX-DOAS measurements observed VCD enhancements of up to  $1 \times 10^{16}$  molec  
471 cm<sup>-2</sup> within this pixel. The averaging due by the large pixel size (24 km×84 km) causes underestimation of the



472 maximum VCDs. Identification of Sarnia-only emissions without error due to horizontal averaging or inclusion of  
473 other sources may require satellite measurements with nadir-viewing pixels centred on Sarnia and/or extremely large  
474 averaging times.

### 475 **3.6 Uncertainties in this Study and Recommended Improvements for Mobile-MAX-DOAS Measurements**

476 Many of the factors that increased the uncertainty in the emission values in this study can be significantly reduced in  
477 future through relatively small changes in the method. The many factors have been addressed in Supplemental  
478 Information (section S7) and summarized in Table S9. Lack of knowledge of the vertical profile of wind-speed  
479 increases uncertainty in Mobile-MAX-DOAS emission estimates since elevated plumes and well-mixed plumes are  
480 transported by winds with typically higher speeds than those near the surface. Future studies could focus on  
481 reducing uncertainty by using measurements from sodar, lidar, tall towers, balloon soundings, or a radio acoustic  
482 meteorological profiler. In this study, uncertainty was increased (18-30% based on sensitivity analysis; see  
483 supplementary S5 & S7) because driving routes could not always include measurements along influx regions (Day  
484 1) due to road proximity to sources or obstructions to the viewing field. Future experiments could measure influx  
485 values while stationary at multiple locations along the upwind region chosen for an unobstructed viewing field. Very  
486 low background trace-gas levels also resulted in zero within error background DSCDs (Fig. 2e). A spectrometer  
487 with a lower limit of detection could solve this issue. Uncertainty in the  $\text{NO}_x$  lifetime was a small contribution to  
488 uncertainty in this study (up to  $\pm 12\%$ ) because the distances and transport times between source and measurement  
489 locations were relatively small ( $< 25$  km). The exception was Day 1 route 1 where uncertainty was up to 30% due to  
490 low wind-speeds. The error contribution of  $\text{NO}_x$  lifetime could be non-trivial if driving routes are far from the  
491 sources (e.g., large cities). This error could also be non-trivial if the lifetime that one assumes does not account for  
492 the multiple factors discussed in Section 3.3. Bias in the emission estimates from an incorrect lifetime could be  
493 avoided by determining  $\text{NO}_x$  lifetimes from photochemical modelling or, for large cities, satellite observations  
494 (Beirle et al., 2011) but taking into account wind speeds (Valin et al., 2013).

### 495 **4 Conclusions**

496 In this study, we combined Mobile-MAX-DOAS techniques with mobile  $\text{NO}_x$  measurements and a modular  
497 meteorological station to measure emissions of  $\text{NO}_x$  and  $\text{SO}_2$  from the Sarnia region, a relatively small  
498 urban/industrial city. Trace-gas VCDs were determined using the  $\text{DSCD}_{\text{offset}}$  method (Wagner et al., 2010) or by



499 fitting measured spectra against a route-local low pollution spectrum. Both methods provided good results, which  
500 suggest that the first method is ideal if there are many hours of measurements while the second method is ideal when  
501 short routes contain low-pollution regions. Average lower limit Mobile-MAX-DOAS emissions of  $\text{NO}_x$  from Sarnia  
502 were measured to be  $1.60 \pm 0.34$  tonnes  $\text{hr}^{-1}$  using 10 m elevation measured wind-speeds. The estimates were larger  
503 than the downscaled 2017 NPRI reported industrial emissions of 0.9 tonnes  $\text{hr}^{-1}$  (Environment and Climate Change  
504 Canada, 2018b) but the NPRI estimate excludes area and mobile emissions. Our lower limit  $\text{SO}_2$  emission  
505 measurement for Sarnia was  $1.81 \pm 0.83$  tonnes  $\text{hr}^{-1}$  using 10 m wind-speeds, which is equal within uncertainty to  
506 the 2017 NPRI value of 1.85 tonnes  $\text{hr}^{-1}$  (Environment and Climate Change Canada, 2018c). Our average lower  
507 limit  $\text{NO}_x$  emission measurement from the NOVA Chemicals Facility was  $0.28 \pm 0.06$  tonnes  $\text{hr}^{-1}$ , the same order of  
508 magnitude as the 2016 NPRI value of 0.14 tonnes  $\text{hr}^{-1}$  (Environment and Climate Change Canada, 2018a).

509 Simultaneous measurements of  $\text{NO-NO}_2\text{-NO}_x$  improved accuracy of  $\text{NO}_x$  emission estimates when plumes of  
510 varying ages were observed. The  $\text{NO}_x$  results from Days 1 and 2 suggest that accurate Mobile-MAX-DOAS  $\text{NO}_x$   
511 emission measurements from routes that observe plumes with differing ages require accurate knowledge of the  
512 localized  $\text{NO}_x/\text{NO}_2$  ratio.

513 The variability in the ratio of the  $\text{NO}_2$  VCDs and mixing ratios indicates that surface  $\text{NO}_2$  mixing ratios cannot be  
514 reliably estimated from  $\text{NO}_2$  VCDs and boundary layer height alone when pollution is emitted from sources of  
515 varying heights and chemical composition. A  $\text{NO}_x$ -analyzer can be an essential component of Mobile-MAX-DOAS  
516  $\text{NO}_2$  measurements. The addition of this instrument allows the method to characterize the boundary layer fully and  
517 accurately estimate  $\text{NO}_x$  emissions from  $\text{NO}_2$  measurements when multiple  $\text{NO}_x$  sources are present and when  
518 transects are sufficiently distant from the sources.

519 The modular meteorological station improved knowledge of local wind essential to identify time periods of low  
520 temporal variability, ensuring low error due to wind estimation. These time periods would have been difficult to  
521 identify with only hourly average or modelled wind data. Accurate knowledge of the vertical wind profile would  
522 significantly enhance the accuracy of the Mobile-MAX-DOAS emission estimates. Future studies could obtain  
523 vertical wind profiles using sodar, lidar, wind-rass, and radiosonde on a weather balloon or local aircraft soundings.



524 Mobile-MAX-DOAS measurements identified significant OMI intrapixel inhomogeneity and observed industrial  
525 pollution enhancements that were poorly captured by the in-situ ground stations. These results suggest that Mobile-  
526 MAX-DOAS has clear advantages in similar industrial regions over other remote sensing techniques used for  
527 estimating emissions (e.g., using aircraft or satellite): higher spatial resolution, the potential for multiple emission  
528 estimates per day (i.e., observations of diurnal trends), and much lower operational costs. Mobile-MAX-DOAS is a  
529 “top-down” low-cost solution for validating bottom-up inventories that compliments in-situ monitoring and has  
530 significant utility in smaller regions with significant emissions where satellite applications are limited. Future  
531 Mobile-MAX-DOAS studies in such regions can focus on measuring temporal trends in emissions.

#### 532 **Author Contributions**

533 ZD conceived of and organized the field campaign with aid from RM. ZD, SB, AK, WF, CC and RM carried out the  
534 experiments in Sarnia. CM modelled conditions for the satellite retrievals of NO<sub>2</sub> in the region of Sarnia, and  
535 provided useful advice. ZD and RM prepared the manuscript, with contributions from all co-authors.

#### 536 **Acknowledgements**

537 This study was completed with collaborative support by the Ontario Ministry of the Environment and Climate  
538 Change. Funding for the study was provided by NSERC, CREATE IACPES and the York University Faculty of  
539 Graduate Studies. The corresponding author would like to thank Mr. Barry Duffey at the Ontario Ministry of  
540 Environment and Climate Change for his support at the project start. We also thank Tony Munoz of OME for his  
541 continued support of our research.

#### 542 **References**

- 543 Aliche, B., Platt, U., and Stutz, J.: Impact of nitrous acid photolysis on the total hydroxyl radical budget during the  
544 limitation of oxidant production/Pianura Padana Produzione di Ozono study in Milan, *J. Geophys. Res.*, 107(D22),  
545 8196, doi:10.1029/2000JD000075, 2002.
- 546 Baray, S., Darlington, A., Gordon, M., Hayden, K. L., Leithead, A., Li, S.-M., Liu, P. S. K., Mittermeier, R. L.,  
547 Moussa, S. G., O’Brien, J., Staebler, R., Wolde, M., Worthy, D. and McLaren, R.: Quantification of methane  
548 sources in the Athabasca Oil Sands Region of Alberta by aircraft mass balance, *Atmospheric Chem. Phys.*, 18(10),  
549 7361–7378, doi:10.5194/acp-18-7361-2018, 2018.
- 550 Beirle, S., Boersma, K. F., Platt, U., Lawrence, M. G. and Wagner, T.: Megacity Emissions and Lifetimes of  
551 Nitrogen Oxides Probed from Space, *Science*, 333(6050), 1737–1739, doi:10.1126/science.1207824, 2011.
- 552 Boersma, K. F., Eskes, H. J., Veefkind, J. P., Brinksma, E. J., Van der A, R. J., Sneep, M., van den Oord, G. H. J.,  
553 Levelt, P. F., Stammes, P., Gleason, J. F. and Bucsela, E. J.: Near-real time retrieval of tropospheric NO<sub>2</sub> from OMI,  
554 *Atmospheric Chem. Phys.*, 7(8), 2103–2118, 2007.



- 555 Bogumil, K., Orphal, J., Homann, T., Voigt, S., Spietz, P., Fleischmann, O. C., Vogel, A., Hartmann, M.,  
556 Kromminga, H., Bovensmann, H., Frerick, J. and Burrows, J. P.: Measurements of molecular absorption spectra  
557 with the SCIAMACHY pre-flight model: instrument characterization and reference data for atmospheric remote-  
558 sensing in the 230-2380 nm region, *J. Photochem. Photobiol. Chem.*, 157(2–3), 167–184, doi:10.1016/S1010-  
559 6030(03)00062-5, 2003.
- 560 Brinksma, E. J., Pinardi, G., Volten, H., Braak, R., Richter, A., Schoenhardt, A., van Roozendaal, M., Fayt, C.,  
561 Hermans, C., Dirksen, R. J., Vlemmix, T., Berkhout, A. J. C., Swart, D. P. J., Oetjen, H., Wittrock, F., Wagner, T.,  
562 Ibrahim, O. W., de Leeuw, G., Moerman, M., Curier, R. L., Celarier, E. A., Cede, A., Knap, W. H., Veeffkind, J. P.,  
563 Eskes, H. J., Allaart, M., Rothe, R., PETERS, A. J. M. and Levelt, P. F.: The 2005 and 2006 DANDELIONS NO<sub>2</sub> and  
564 aerosol intercomparison campaigns, *J. Geophys. Res.-Atmospheres*, 113(D16), D16S46,  
565 doi:10.1029/2007JD008808, 2008.
- 566 Brown, S. S., Dube, W. P., Karamchandani, P., Yarwood, G., Peischl, J., Ryerson, T. B., Neuman, J. A., Nowak, J.  
567 B., Holloway, J. S., Washenfelder, R. A., Brock, C. A., Frost, G. J., Trainer, M., Parrish, D. D., Fehsenfeld, F. C.  
568 and Ravishankara, A. R.: Effects of NO<sub>x</sub> control and plume mixing on nighttime chemical processing of plumes  
569 from coal-fired power plants, *J. Geophys. Res.-Atmospheres*, 117, D07304, doi:10.1029/2011JD016954, 2012.
- 570 Canada, E. and C. C. and Canada, E. and C. C.: Using and interpreting data from the National Pollutant Release  
571 Inventory, aem [online] Available from: [https://www.canada.ca/en/environment-climate-change/services/national-](https://www.canada.ca/en/environment-climate-change/services/national-pollutant-release-inventory/using-interpreting-data.html)  
572 [pollutant-release-inventory/using-interpreting-data.html](https://www.canada.ca/en/environment-climate-change/services/national-pollutant-release-inventory/using-interpreting-data.html) (Accessed 1 August 2018), 2015.
- 573 Dragomir, C. M., Constantin, D.-E., Voiculescu, M., Georgescu, L. P., Merlaud, A. and Van Roozendaal, M.:  
574 Modeling results of atmospheric dispersion of NO<sub>2</sub> in an urban area using METI-LIS and comparison with  
575 coincident mobile DOAS measurements, *Atmos. Pollut. Res.*, 6(3), 503–510, doi:10.5094/APR.2015.056, 2015.
- 576 Dunlea, E. J., Herndon, S. C., Nelson, D. D., Volkamer, R. M., San Martini, F., Sheehy, P. M., Zahniser, M. S.,  
577 Shorter, J. H., Wormhoudt, J. C., Lamb, B. K., Allwine, E. J., Gaffney, J. S., Marley, N. A., Grutter, M., Marquez,  
578 C., Blanco, S., Cardenas, B., Retama, A., Ramos Villegas, C. R., Kolb, C. E., Molina, L. T., and Molina, M. J.:  
579 Evaluation of nitrogen dioxide chemiluminescence monitors in a polluted urban environment, *Atmos. Chem. Phys.*,  
580 7, 2691-2704, 10.5194/acp-7-2691-2007, 2007.
- 581 Environment and Climate Change Canada: NPRI Data Search - Facility and Substance Information - NOVA  
582 Chemicals (Canada) Ltd. - Corunna Site 2017, [online] Available from: [https://pollution-waste.canada.ca/national-](https://pollution-waste.canada.ca/national-release-inventory/archives/index.cfm?do=facility_substance_summary&lang=en&opt_npri_id=0000001776&opt_report_year=2017)  
583 [release-](https://pollution-waste.canada.ca/national-release-inventory/archives/index.cfm?do=facility_substance_summary&lang=en&opt_npri_id=0000001776&opt_report_year=2017)  
584 [inventory/archives/index.cfm?do=facility\\_substance\\_summary&lang=en&opt\\_npri\\_id=0000001776&opt\\_report\\_ye](https://pollution-waste.canada.ca/national-release-inventory/archives/index.cfm?do=facility_substance_summary&lang=en&opt_npri_id=0000001776&opt_report_year=2017)  
585 [ar=2017](https://pollution-waste.canada.ca/national-release-inventory/archives/index.cfm?do=facility_substance_summary&lang=en&opt_npri_id=0000001776&opt_report_year=2017) (Accessed 17 September 2018a), 2018.
- 586 Environment and Climate Change Canada: NPRI Data Search - Facility Search Results Nitrogen oxides (expressed  
587 as NO<sub>2</sub>) (11104-93-1), [online] Available from: [https://pollution-waste.canada.ca/national-release-](https://pollution-waste.canada.ca/national-release-inventory/archives/index.cfm?do=results&process=true&lang=en&opt_report_year=2017&opt_facility_name=&opt_npri_id=&opt_cas_name=11104-93-1&opt_cas_num=&opt_province=&opt_postal_code=&opt_urban_center=&opt_province_comm=&opt_naics6=&opt_naics3=&opt_naics4=&opt_nai6code=&opt_csic=&opt_media=all&submit=Submit)  
588 [inventory/archives/index.cfm?do=results&process=true&lang=en&opt\\_report\\_year=2017&opt\\_facility\\_name=&opt](https://pollution-waste.canada.ca/national-release-inventory/archives/index.cfm?do=results&process=true&lang=en&opt_report_year=2017&opt_facility_name=&opt_npri_id=&opt_cas_name=11104-93-1&opt_cas_num=&opt_province=&opt_postal_code=&opt_urban_center=&opt_province_comm=&opt_naics6=&opt_naics3=&opt_naics4=&opt_nai6code=&opt_csic=&opt_media=all&submit=Submit)  
589 [\\_npri\\_id=&opt\\_cas\\_name=11104-93-](https://pollution-waste.canada.ca/national-release-inventory/archives/index.cfm?do=results&process=true&lang=en&opt_report_year=2017&opt_facility_name=&opt_npri_id=&opt_cas_name=11104-93-1&opt_cas_num=&opt_province=&opt_postal_code=&opt_urban_center=&opt_province_comm=&opt_naics6=&opt_naics3=&opt_naics4=&opt_nai6code=&opt_csic=&opt_media=all&submit=Submit)  
590 [1&opt\\_cas\\_num=&opt\\_province=&opt\\_postal\\_code=&opt\\_urban\\_center=&opt\\_province\\_comm=&opt\\_naics6=&o](https://pollution-waste.canada.ca/national-release-inventory/archives/index.cfm?do=results&process=true&lang=en&opt_report_year=2017&opt_facility_name=&opt_npri_id=&opt_cas_name=11104-93-1&opt_cas_num=&opt_province=&opt_postal_code=&opt_urban_center=&opt_province_comm=&opt_naics6=&opt_naics3=&opt_naics4=&opt_nai6code=&opt_csic=&opt_media=all&submit=Submit)  
591 [pt\\_naics3=&opt\\_naics4=&opt\\_nai6code=&opt\\_csic=&opt\\_media=all&submit=Submit](https://pollution-waste.canada.ca/national-release-inventory/archives/index.cfm?do=results&process=true&lang=en&opt_report_year=2017&opt_facility_name=&opt_npri_id=&opt_cas_name=11104-93-1&opt_cas_num=&opt_province=&opt_postal_code=&opt_urban_center=&opt_province_comm=&opt_naics6=&opt_naics3=&opt_naics4=&opt_nai6code=&opt_csic=&opt_media=all&submit=Submit) (Accessed 17 September  
592 2018b), 2018.
- 593 Environment and Climate Change Canada: NPRI Data Search - Facility Search Results Sulphur Dioxide (7446-09-  
594 5), [online] Available from: [https://pollution-waste.canada.ca/national-release-](https://pollution-waste.canada.ca/national-release-inventory/archives/index.cfm?do=results&process=true&lang=en&opt_report_year=2017&opt_facility_name=&opt_npri_id=&opt_cas_name=7446-09-5&opt_cas_num=&opt_province=&opt_postal_code=&opt_urban_center=&opt_province_comm=&opt_naics6=&opt_naics3=&opt_naics4=&opt_nai6code=&opt_csic=&opt_media=all&submit=Submit)  
595 [inventory/archives/index.cfm?do=results&process=true&lang=en&opt\\_report\\_year=2017&opt\\_facility\\_name=&opt](https://pollution-waste.canada.ca/national-release-inventory/archives/index.cfm?do=results&process=true&lang=en&opt_report_year=2017&opt_facility_name=&opt_npri_id=&opt_cas_name=7446-09-5&opt_cas_num=&opt_province=&opt_postal_code=&opt_urban_center=&opt_province_comm=&opt_naics6=&opt_naics3=&opt_naics4=&opt_nai6code=&opt_csic=&opt_media=all&submit=Submit)  
596 [\\_npri\\_id=&opt\\_cas\\_name=7446-09-](https://pollution-waste.canada.ca/national-release-inventory/archives/index.cfm?do=results&process=true&lang=en&opt_report_year=2017&opt_facility_name=&opt_npri_id=&opt_cas_name=7446-09-5&opt_cas_num=&opt_province=&opt_postal_code=&opt_urban_center=&opt_province_comm=&opt_naics6=&opt_naics3=&opt_naics4=&opt_nai6code=&opt_csic=&opt_media=all&submit=Submit)  
597 [5&opt\\_cas\\_num=&opt\\_province=&opt\\_postal\\_code=&opt\\_urban\\_center=&opt\\_province\\_comm=&opt\\_naics6=&o](https://pollution-waste.canada.ca/national-release-inventory/archives/index.cfm?do=results&process=true&lang=en&opt_report_year=2017&opt_facility_name=&opt_npri_id=&opt_cas_name=7446-09-5&opt_cas_num=&opt_province=&opt_postal_code=&opt_urban_center=&opt_province_comm=&opt_naics6=&opt_naics3=&opt_naics4=&opt_nai6code=&opt_csic=&opt_media=all&submit=Submit)  
598 [pt\\_naics3=&opt\\_naics4=&opt\\_nai6code=&opt\\_csic=&opt\\_media=all&submit=Submit](https://pollution-waste.canada.ca/national-release-inventory/archives/index.cfm?do=results&process=true&lang=en&opt_report_year=2017&opt_facility_name=&opt_npri_id=&opt_cas_name=7446-09-5&opt_cas_num=&opt_province=&opt_postal_code=&opt_urban_center=&opt_province_comm=&opt_naics6=&opt_naics3=&opt_naics4=&opt_nai6code=&opt_csic=&opt_media=all&submit=Submit) (Accessed 17 September  
599 2018c), 2018.



- 600 Environment and Climate Change Canada: NPRI Facility Search Results - Volatile Organic Compounds (VOCs)  
601 (NA-M16), [online] Available from: [https://pollution-waste.canada.ca/national-release-](https://pollution-waste.canada.ca/national-release-inventory/archives/index.cfm?do=results&process=true&lang=en&opt_report_year=2017&opt_facility_name=&opt_npri_id=&opt_cas_name=NA+-+M16&opt_cas_num=&opt_province=&opt_postal_code=&opt_urban_center=&opt_province_comm=&opt_naics6=&opt_naics3=&opt_naics4=&opt_nai6code=&opt_csic=&opt_media=all&submit=Submit)  
602 [inventory/archives/index.cfm?do=results&process=true&lang=en&opt\\_report\\_year=2017&opt\\_facility\\_name=&opt](https://pollution-waste.canada.ca/national-release-inventory/archives/index.cfm?do=results&process=true&lang=en&opt_report_year=2017&opt_facility_name=&opt_npri_id=&opt_cas_name=NA+-+M16&opt_cas_num=&opt_province=&opt_postal_code=&opt_urban_center=&opt_province_comm=&opt_naics6=&opt_naics3=&opt_naics4=&opt_nai6code=&opt_csic=&opt_media=all&submit=Submit)  
603 [\\_npri\\_id=&opt\\_cas\\_name=NA+-](https://pollution-waste.canada.ca/national-release-inventory/archives/index.cfm?do=results&process=true&lang=en&opt_report_year=2017&opt_facility_name=&opt_npri_id=&opt_cas_name=NA+-+M16&opt_cas_num=&opt_province=&opt_postal_code=&opt_urban_center=&opt_province_comm=&opt_naics6=&opt_naics3=&opt_naics4=&opt_nai6code=&opt_csic=&opt_media=all&submit=Submit)  
604 [+M16&opt\\_cas\\_num=&opt\\_province=&opt\\_postal\\_code=&opt\\_urban\\_center=&opt\\_province\\_comm=&opt\\_naics6](https://pollution-waste.canada.ca/national-release-inventory/archives/index.cfm?do=results&process=true&lang=en&opt_report_year=2017&opt_facility_name=&opt_npri_id=&opt_cas_name=NA+-+M16&opt_cas_num=&opt_province=&opt_postal_code=&opt_urban_center=&opt_province_comm=&opt_naics6=&opt_naics3=&opt_naics4=&opt_nai6code=&opt_csic=&opt_media=all&submit=Submit)  
605 [=&opt\\_naics3=&opt\\_naics4=&opt\\_nai6code=&opt\\_csic=&opt\\_media=all&submit=Submit](https://pollution-waste.canada.ca/national-release-inventory/archives/index.cfm?do=results&process=true&lang=en&opt_report_year=2017&opt_facility_name=&opt_npri_id=&opt_cas_name=NA+-+M16&opt_cas_num=&opt_province=&opt_postal_code=&opt_urban_center=&opt_province_comm=&opt_naics6=&opt_naics3=&opt_naics4=&opt_nai6code=&opt_csic=&opt_media=all&submit=Submit) (Accessed 17  
606 September 2018d), 2018.
- 607 Finlayson-Pitts, B. J. and Pitts, J.N.: Chemistry of the Upper and Lower Atmosphere, Academic Press, San Diego  
608 CA, 969 pp., 2000.
- 609 Friess, U., Monks, P. S., Remedios, J. J., Rozanov, A., Sinreich, R., Wagner, T. and Platt, U.: MAX-DOAS O4  
610 measurements: A new technique to derive information on atmospheric aerosols: 2. Modeling studies, *J. Geophys.*  
611 *Res.-Atmospheres*, 111(D14), D14203, doi:10.1029/2005JD006618, 2006.
- 612 Gordon, M., Li, S.-M., Staebler, R., Darlington, A., Hayden, K., O'Brien, J. and Wolde, M.: Determining air  
613 pollutant emission rates based on mass balance using airborne measurement data over the Alberta oil sands  
614 operations, *Atmos. Meas. Tech.*, 8(9), 3745–3765, doi:10.5194/amt-8-3745-2015, 2015.
- 615 Halla, J. D., Wagner, T., Beirle, S., Brook, J. R., Hayden, K. L., O'Brien, J. M., Ng, A., Majonis, D., Wenig, M. O.  
616 and McLaren, R.: Determination of tropospheric vertical columns of NO<sub>2</sub> and aerosol optical properties in a rural  
617 setting using MAX-DOAS, *Atmos. Chem. Phys.*, 11(23), 12475–12498, doi:10.5194/acp-11-12475-2011, 2011.
- 618 Heckel, A., Richter, A., Tarsu, T., Wittrock, F., Hak, C., Pundt, I., Junkermann, W. and Burrows, J. P.: MAX-DOAS  
619 measurements of formaldehyde in the Po-Valley, *Atmos. Chem. Phys.*, 5, 909–918, doi:10.5194/acp-5-909-2005,  
620 2005.
- 621 Heckel, A., Kim, S.-W., Frost, G. J., Richter, A., Trainer, M. and Burrows, J. P.: Influence of low spatial resolution  
622 a priori data on tropospheric NO<sub>2</sub> satellite retrievals, *Atmos. Meas. Tech.*, 4(9), 1805–1820, doi:10.5194/amt-4-  
623 1805-2011, 2011.
- 624 Honninger, G. and Platt, U.: Observations of BrO and its vertical distribution during surface ozone depletion at  
625 Alert, *Atmos. Environ.*, 36(15–16), 2481–2489, doi:10.1016/S1352-2310(02)00104-8, 2002.
- 626 Honninger, G., von Friedeburg, C. and Platt, U.: Multi axis differential optical absorption spectroscopy (MAX-  
627 DOAS), *Atmos. Chem. Phys.*, 4, 231–254, 2004.
- 628 Huang, M., Bowman, K. W., Carmichael, G. R., Chai, T., Pierce, R. B., Worden, J. R., Luo, M., Pollack, I. B.,  
629 Ryerson, T. B., Nowak, J. B., Neuman, J. A., Roberts, J. M., Atlas, E. L. and Blake, D. R.: Changes in nitrogen  
630 oxides emissions in California during 2005–2010 indicated from top-down and bottom-up emission estimates, *J.*  
631 *Geophys. Res.-Atmospheres*, 119(22), 12928–12952, doi:10.1002/2014JD022268, 2014.
- 632 Ialongo, I., Hakkarainen, J., Hyttinen, N., Jalkanen, J.-P., Johansson, L., Boersma, K. F., Krotkov, N. and  
633 Tamminen, J.: Characterization of OMI tropospheric NO<sub>2</sub> over the Baltic Sea region, *Atmos. Chem. Phys.*, 14(15),  
634 7795–7805, doi:10.5194/acp-14-7795-2014, 2014.
- 635 Ialongo, I., Herman, J., Krotkov, N., Lamsal, L., Boersma, K. F., Hovila, J. and Tamminen, J.: Comparison of OMI  
636 NO<sub>2</sub> observations and their seasonal and weekly cycles with ground-based measurements in Helsinki, *Atmos. Meas.*  
637 *Tech.*, 9(10), 5203–5212, doi:10.5194/amt-9-5203-2016, 2016.
- 638 Ibrahim, O., Shaiganfar, R., Sinreich, R., Stein, T., Platt, U. and Wagner, T.: Car MAX-DOAS measurements  
639 around entire cities: quantification of NO<sub>x</sub> emissions from the cities of Mannheim and Ludwigshafen (Germany),  
640 *Atmos. Meas. Tech.*, 3(3), 709–721, doi:10.5194/amt-3-709-2010, 2010.



- 641 Irie, H., Kanaya, Y., Akimoto, H., Iwabuchi, H., Shimizu, A. and Aoki, K.: First retrieval of tropospheric aerosol  
642 profiles using MAX-DOAS and comparison with lidar and sky radiometer measurements, *Atmos. Chem. Phys.*,  
643 8(2), 341–350, doi:10.5194/acp-8-341-2008, 2008.
- 644 Kim, N. K., Kim, Y. P., Morino, Y., Kurokawa, J. and Ohara, T.: Verification of NO<sub>x</sub> emission inventories over  
645 North Korea, *Environ. Pollut.*, 195, 236–244, doi:10.1016/j.envpol.2014.06.034, 2014.
- 646 Leighton, P. A.: *Photochemistry of air pollution.* --, Academic Press, New York., 1961.
- 647 Liu, F., Beirle, S., Zhang, Q., Doerner, S., He, K. and Wagner, T.: NO<sub>x</sub> lifetimes and emissions of cities and power  
648 plants in polluted background estimated by satellite observations, *Atmos. Chem. Phys.*, 16(8), 5283–5298,  
649 doi:10.5194/acp-16-5283-2016, 2016.
- 650 McLinden, C. A., Fioletov, V., Boersma, K. F., Krotkov, N., Sioris, C. E., Veefkind, J. P. and Yang, K.: Air quality  
651 over the Canadian oil sands: A first assessment using satellite observations, *Geophys. Res. Lett.*, 39, L04804,  
652 doi:10.1029/2011GL050273, 2012.
- 653 Ministry of the Environment and Climate Change: Air Quality in Ontario 2014 Report, [online] Available from:  
654 <http://www.airqualityontario.com/downloads/AirQualityInOntarioReportAndAppendix2014.pdf> (Accessed 25  
655 August 2016), 2015.
- 656 Ministry of the Environment and Climate Change: Air Quality in Ontario 2016 Report., 2016.
- 657 Nunnermacker, L. J., Kleinman, L. I., Imre, D., Daum, P. H., Lee, Y.-N., Lee, J. H., Springston, S. R., Newman, L.  
658 and Gillani, N.: NO<sub>y</sub> lifetimes and O<sub>3</sub> production efficiencies in urban and power plant plumes: Analysis of field  
659 data, *J. Geophys. Res. Atmospheres*, 105(D7), 9165–9176, doi:10.1029/1999JD900753, 2000.
- 660 Oiamo, T. H., Luginaah, I. N., Atari, D. O. and Gorey, K. M.: Air pollution and general practitioner access and  
661 utilization: a population based study in Sarnia, 'Chemical Valley,' Ontario, *Environ. Health*, 10, doi:10.1186/1476-  
662 069X-10-71, 2011.
- 663 Platt, U., Perner, D. and Patz, H.: Simultaneous Measurement of Atmospheric CH<sub>2</sub>O, O<sub>3</sub>, and NO<sub>2</sub> by Differential  
664 Optical-Absorption, *J. Geophys. Res.-Oceans Atmospheres*, 84(NC10), 6329–6335, doi:10.1029/JC084iC10p06329,  
665 1979.
- 666 Platt, U., Perner, D., Harris, G.W., Winer, A. M., and Pitts Jr., J. N.: Observations of nitrous acid in an urban  
667 atmosphere by differential optical absorption, *Nature*, 285, 312–314, 1980.
- 668 Platt, U., Stutz, J., Springer E-books - York University and SpringerLink (Online service): Differential optical  
669 absorption spectroscopy: principles and applications, Springer Verlag, Berlin. [online] Available from:  
670 <http://www.library.yorku.ca/eresolver/?id=1261530>, 2008.
- 671 Rivera, C., Mellqvist, J., Samuelsson, J., Lefer, B., Alvarez, S., and Patel, M. R.: Quantification of NO<sub>2</sub> and SO<sub>2</sub>  
672 emissions from the Houston Ship Channel and Texas City industrial areas during the 2006 Texas Air Quality Study,  
673 *Journal of Geophysical Research: Atmospheres*, 115, 10.1029/2009jd012675, 2010.
- 674 Ryerson, T. B., Trainer, M., Angevine, W. M., Brock, C. A., Dissly, R. W., Fehsenfeld, F. C., Frost, G. J., Goldan,  
675 P. D., Holloway, J. S., Hubler, G., Jakoubek, R. O., Kuster, W. C., Neuman, J. A., Nicks, D. K., Parrish, D. D.,  
676 Roberts, J. M., Sueper, D. T., Atlas, E. L., Donnelly, S. G., Flocke, F., Fried, A., Potter, W. T., Schauffler, S.,  
677 Stroud, V., Weinheimer, A. J., Wert, B. P., Wiedinmyer, C., Alvarez, R. J., Banta, R. M., Darby, L. S. and Senff, C.  
678 J.: Effect of petrochemical industrial emissions of reactive alkenes and NO<sub>x</sub> on tropospheric ozone formation in  
679 Houston, Texas, *J. Geophys. Res.-Atmospheres*, 108(D8), 4249, doi:10.1029/2002JD003070, 2003.
- 680 Seinfeld, J. H. and Pandis, S. N.: *Atmospheric Chemistry and Physics: From Air Pollution to Climate Change*, John  
681 Wiley & Sons., 2006.



- 682 Shabbir, Y., Khokhar, M. F., Shaiganfar, R. and Wagner, T.: Spatial variance and assessment of nitrogen dioxide  
683 pollution in major cities of Pakistan along N5-Highway, *J. Environ. Sci.*, 43(Supplement C), 4–14,  
684 doi:10.1016/j.jes.2015.04.038, 2016.
- 685 Shaiganfar, R., Beirle, S., Sharma, M., Chauhan, A., Singh, R. P. and Wagner, T.: Estimation of NO<sub>x</sub> emissions  
686 from Delhi using Car MAX-DOAS observations and comparison with OMI satellite data, *Atmos. Chem. Phys.*,  
687 11(21), 10871–10887, doi:10.5194/acp-11-10871-2011, 2011.
- 688 Shaiganfar, R., Beirle, S., Petetin, H., Zhang, Q., Beekmann, M. and Wagner, T.: New concepts for the comparison  
689 of tropospheric NO<sub>2</sub> column densities derived from car-MAX-DOAS observations, OMI satellite observations and  
690 the regional model CHIMERE during two MEGAPOLI campaigns in Paris 2009/10, *Atmos. Meas. Tech.*, 8(7),  
691 2827–2852, doi:10.5194/amt-8-2827-2015, 2015.
- 692 Shaiganfar, R., Beirle, S., van der Gon, H. D., Jonkers, S., Kuenen, J., Petetin, H., Zhang, Q., Beekmann, M. and  
693 Wagner, T.: Estimation of the Paris NO<sub>x</sub> emissions from mobile MAX-DOAS observations and CHIMERE model  
694 simulations during the MEGAPOLI campaign using the closed integral method, *Atmos. Chem. Phys.*, 17(12), 7853–  
695 7890, doi:10.5194/acp-17-7853-2017, 2017.
- 696 Tokarek, T. W., Odam-Ankrah, C. A., Huo, J. A., McLaren, R., Lee, A. K. Y., Adam, M. G., Willis, M. D., Abbatt,  
697 J. P. D., Mihele, C., Darlington, A., Mittermeier, R. L., Strawbridge, K., Hayden, K. L., Olfert, J. S., Schnitzler, E.  
698 G., Brownsey, D. K., Assad, F. V., Wentworth, G. R., Tevlin, A. G., Worthy, D. E. J., Li, S.-M., Liggio, J., Brook, J.  
699 R. and Osthoff, H. D.: Principal component analysis of summertime ground site measurements in the Athabasca oil  
700 sands with a focus on analytically unresolved intermediate volatility organic compounds, *Atmos. Chem. Phys.*,  
701 2018, 17819–17841, doi:10.5194/acp-18-17819-2018, 2018.
- 702 United States EPA: Air Pollutant Report | ECHO | US EPA, Air Pollut. Rep. [online] Available from:  
703 <https://echo.epa.gov/air-pollutant-report?fid=110000404740> (Accessed 2 August 2018), 2018.
- 704 Valin, L. C., Russell, A. R. and Cohen, R. C.: Variations of OH radical in an urban plume inferred from NO<sub>2</sub> column  
705 measurements, *Geophys. Res. Lett.*, 40(9), 1856–1860, doi:10.1002/grl.50267, 2013.
- 706 Wagner, T., Dix, B., von Friedeburg, C., Friess, U., Sanghavi, S., Sinreich, R. and Platt, U.: MAX-DOAS O<sub>4</sub>  
707 measurements: A new technique to derive information on atmospheric aerosols - Principles and information content,  
708 *J. Geophys. Res.-Atmospheres*, 109(D22), D22205, doi:10.1029/2004JD004904, 2004.
- 709 Wagner, T., Ibrahim, O., Shaiganfar, R. and Platt, U.: Mobile MAX-DOAS observations of tropospheric trace gases,  
710 *Atmos. Meas. Tech.*, 3(1), 129–140, 2010.
- 711 Wagner, T., Beirle, S., Brauers, T., Deutschmann, T., Friess, U., Hak, C., Halla, J. D., Heue, K. P., Junkermann, W.,  
712 Li, X., Platt, U. and Pundt-Gruber, I.: Inversion of tropospheric profiles of aerosol extinction and HCHO and NO<sub>2</sub>  
713 mixing ratios from MAX-DOAS observations in Milano during the summer of 2003 and comparison with  
714 independent data sets, *Atmos. Meas. Tech.*, 4(12), 2685–2715, doi:10.5194/amt-4-2685-2011, 2011.
- 715 Wiegand, A. N. and Bofinger, N. D.: Review of empirical methods for the calculation of the diurnal NO<sub>2</sub> photolysis  
716 rate coefficient, *Atmos. Environ.*, 34(1), 99–108, doi:10.1016/S1352-2310(99)00294-0, 2000.
- 717 Wu, F., Li, A., Xie, P., Chen, H., Hu, Z., Zhang, Q., Liu, J. and Liu, W.: Emission Flux Measurement Error with a  
718 Mobile DOAS System and Application to NO<sub>x</sub> Flux Observations, *Sensors*, 17(2), doi:10.3390/s17020231, 2017.

719



720 **Table 1** Daily meteorological conditions, number of routes and time period of routes driven. Wind-speed from  
721 SLEA LaSalle Road; Temperature and Relative Humidity from portable meteorological station Day 1 and Day 2 and  
722 from Moore Line station Day 2.

| Date      | Number of Routes Driven | Measurement Local Time Period | Average Wind-speed (km hr <sup>-1</sup> ) | Prevailing Wind-Direction | Average Temperature (°C) | Average Relative Humidity (%) | Emission Area Measured             |
|-----------|-------------------------|-------------------------------|---|---------------------------|--------------------------|-------------------------------|------------------------------------|
| 3/21/2017 | 4                       | 10:26-13:16                   | 15  | Westerly                  | 10                       | 50                            | City of Sarnia                     |
| 3/22/2017 | 1                       | 17:22-17:41                   | 8   | Northerly                 | -3                       | 52                            | City of Sarnia                     |
| 3/23/2017 | 2                       | 11:10-11:57                   | 15  | Southerly                 | 1                        | 42                            | NOVA Chemicals Industries Facility |

723



724 **Table 2** NO<sub>x</sub>/NO<sub>2</sub> ratios for routes driven.

| Date      | Day's  |              | Measurement |              |        |
|-----------|--------|--------------|-------------|--------------|--------|
|           | Route  | Local Time   | Number of   | Average ± 1σ | Median |
|           | Number | Period       | Points      |              |        |
| 3/21/2017 | 1      | 10:26-11:06  | 37          | 1.53±0.12    | 1.49   |
| 3/21/2017 | 2      | 11:22-11:45  | 23          | 1.45±0.06    | 1.44   |
| 3/21/2017 | 3      | 12:09-12:28  | 18          | 1.36±0.07    | 1.37   |
| 3/21/2017 | 4      | 12:34-13:16  | 24          | 1.29±0.06    | 1.31   |
| 3/22/2017 | 1      | 17:22-17:41  | 10          | 1.49±0.53    | 1.30   |
| 3/22/2017 | 1      | 17:22-17:41* | 9           | 1.32±0.08    | 1.30   |
| 3/23/2017 | 1      | 11:10-11:19  | 5           | 1.39±0.09    | 1.39   |
| 3/23/2017 | 2      | 11:42-11:57  | 9           | 1.46±0.17    | 1.52   |

725 The 3/22/2017 17:22-17:41\* data had the peak NO<sub>x</sub>/NO<sub>2</sub> value removed.

726



727 **Table 3** Calculated Leighton Ratios for selected plume maximums on Day 1 and 2.

| Date       | Local Time | $J_{\text{NO}_2}$<br>( $\times 10^{-3} \text{ s}^{-1}$ ) | Solar<br>Irradiance<br>( $\text{W m}^{-2}$ ) | Solar Zenith<br>Angle | $\text{O}_3$ mixing<br>ratio (ppb) | Measured<br>$\text{NO}_2/\text{NO}$<br>(ppb $\text{ppb}^{-1}$ ) | Calculated<br>Leighton<br>Ratio |
|------------|------------|--|--|-----------------------|------------------------------------|---|---------------------------------|
| 21/03/2017 | 11:00      | 5.23   | 564  | 35                    | 18                                 | 1.7   | 1.61                            |
| 21/03/2017 | 11:30      | 5.65   | 600  | 40                    | 23                                 | 2.2   | 1.76                            |
| 21/03/2017 | 12:15      | 6.44   | 675  | 43                    | 23                                 | 2.2   | 2.01                            |
| 22/03/2017 | 17:28      | 2.71   | 300  | 23                    | 10                                 | 0.5   | 0.44                            |

728

729



730 **Table 4** Lower limit NO<sub>x</sub> Emission Estimates from 10 m elevation wind-speeds.

| Date       | Emission Source | Daily Route Number | Lower-limit NO <sub>x</sub> (tonnes hr <sup>-1</sup> ) | NPRI NO <sub>x</sub> (tonnes hr <sup>-1</sup> ) |
|------------|-----------------|--------------------|--|---|
| 21/03/2017 | Sarnia          | 1                  | 1.6±0.8  | 0.9   |
| 21/03/2017 | Sarnia          | 2                  | 1.2±0.5  | 0.9   |
| 21/03/2017 | Sarnia          | 3                  | 1.4±0.5  | 0.9   |
| 22/03/2017 | Sarnia          | 1                  | 1.5±0.6  | 0.9   |
| 22/03/2017 | Sarnia          | 1*                 | 2.2±0.8  | 0.9   |
| 23/03/2017 | NovaChem        | 1                  | 0.27±0.1   | 0.14  |
| 23/03/2017 | NovaChem        | 2                  | 0.29±0.1   | 0.14  |

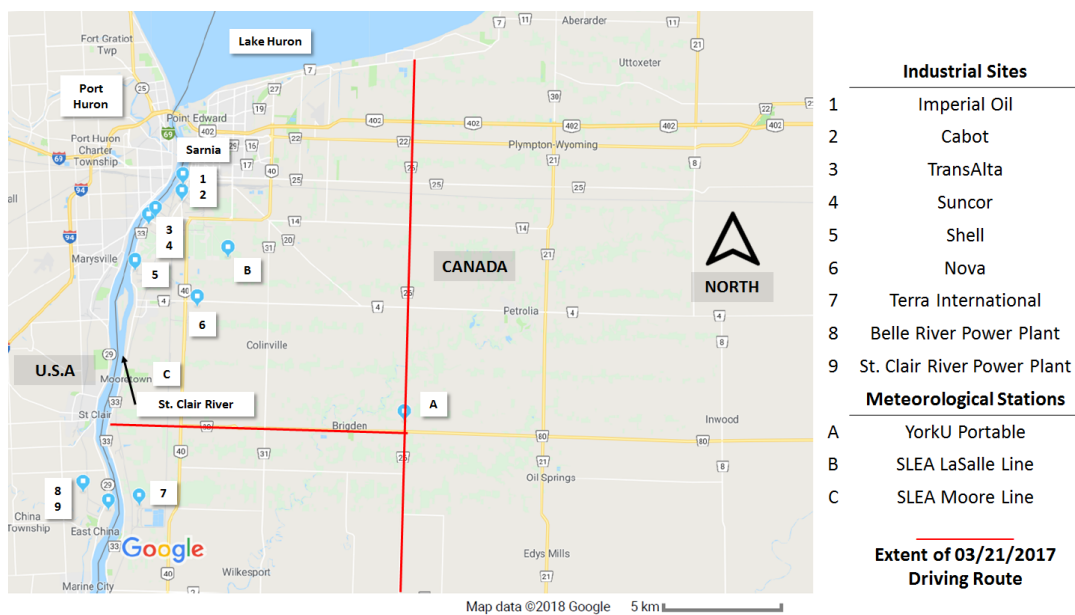
731 \* calculated using individual NO<sub>x</sub>/NO<sub>2</sub> ratios.



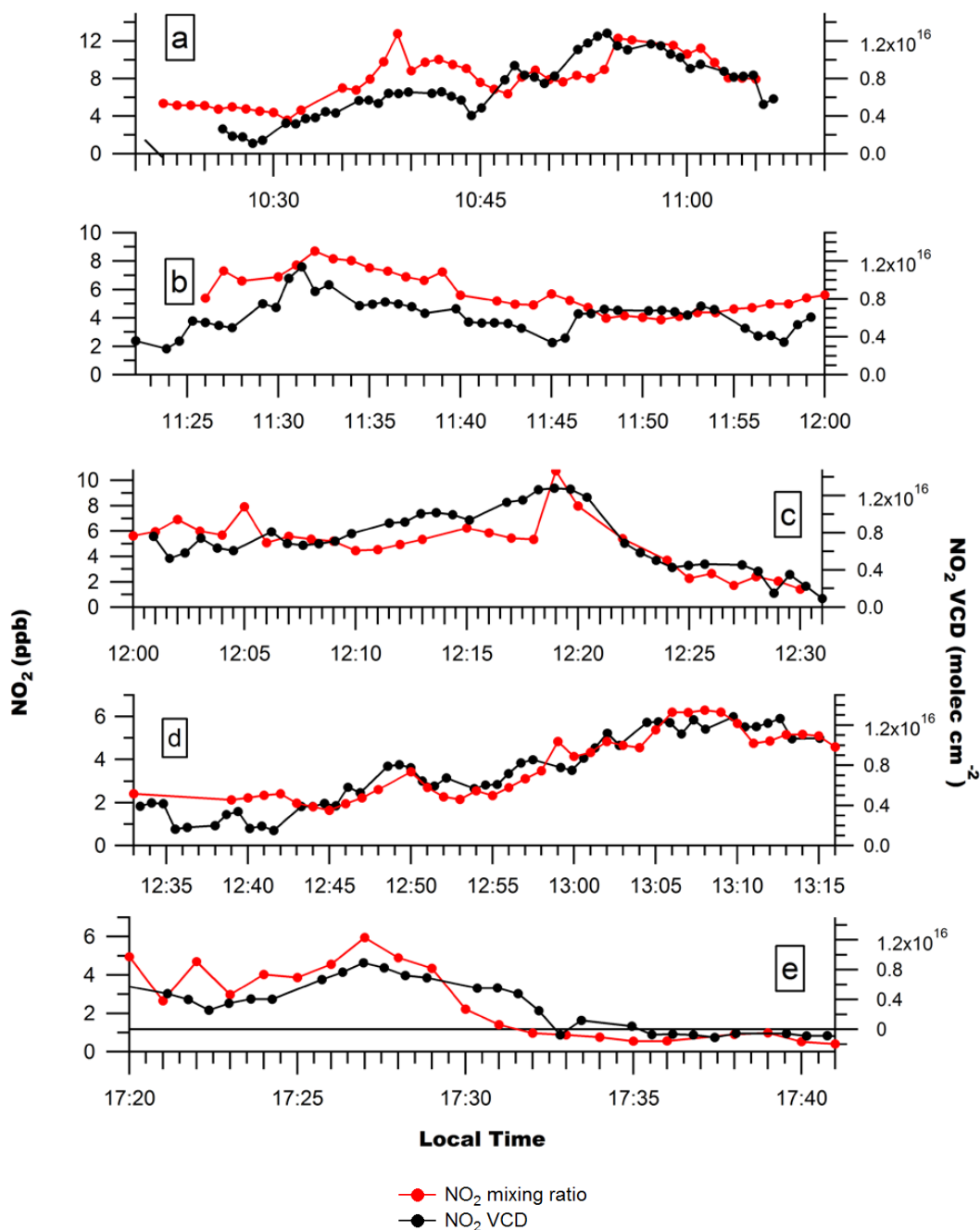
732 **Table 5** Average NO<sub>x</sub> emission estimates from Mobile MAX\_DOAS using 10 m wind-speeds and from NPRI.

|                                    | Gas             | Lower Limit Emission Estimate<br>(tonnes hr <sup>-1</sup> ) | 2017 NPRI Value<br>(tonnes hr <sup>-1</sup> ) |
|------------------------------------|-----------------|---|---|
| Sarnia                             | NO <sub>x</sub> | 1.60±0.34   | 0.9   |
| Sarnia                             | SO <sub>2</sub> | 1.81±0.83   | 1.85  |
| NOVA<br>Chemicals-<br>Corunna Site | NO <sub>x</sub> | 0.28±0.06   | 0.14  |

733



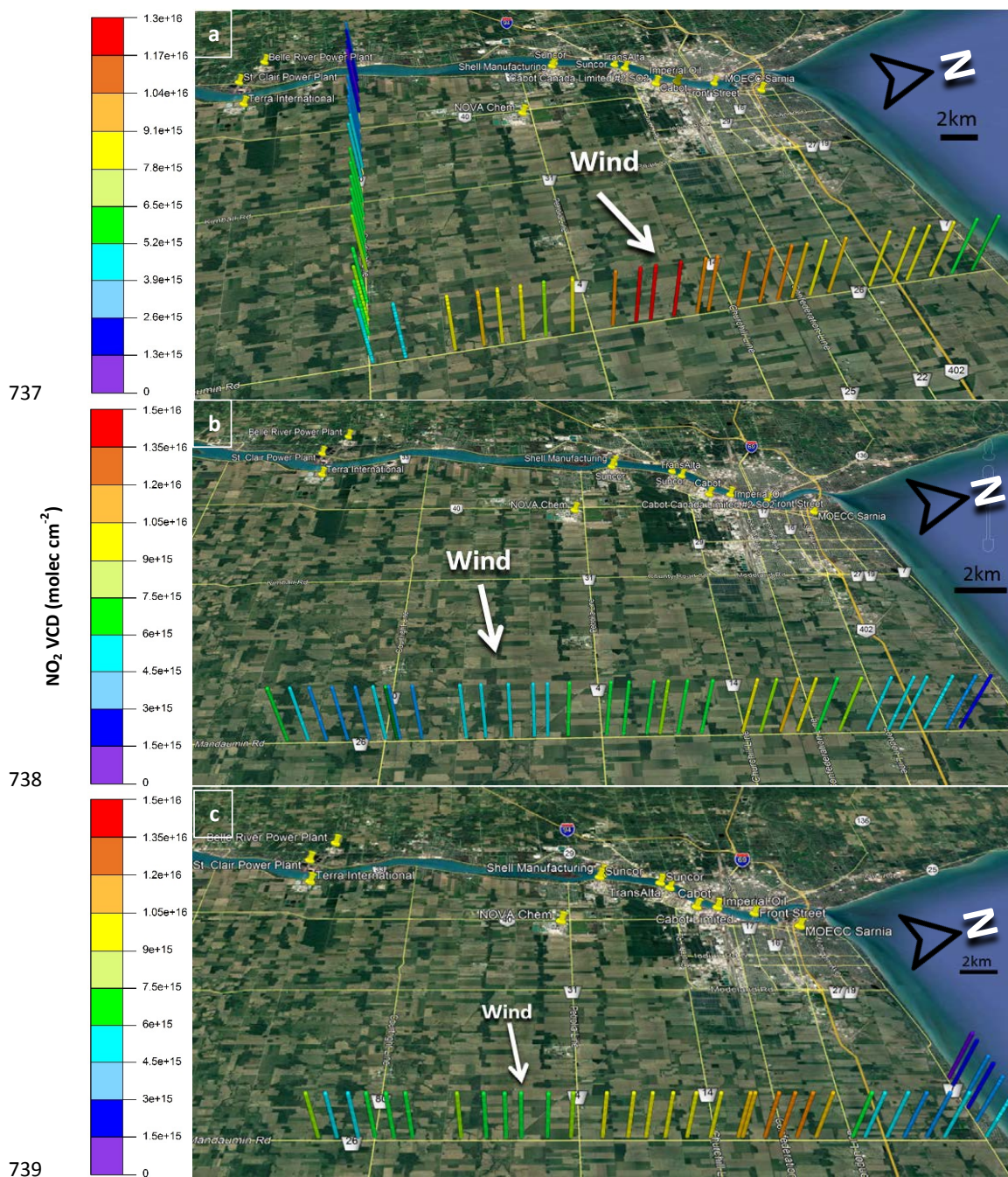
734 **Figure 1** Location of industrial NO<sub>x</sub> and SO<sub>2</sub> emission sources and meteorological stations in the Sarnia area.



735

736

**Figure 2**  $\text{NO}_2$  mixing ratios and  $\text{NO}_2$  VCDs along routes 1-4 on Day 1 (a) – (d) and route 1 on Day 2 (e).



737

738

739

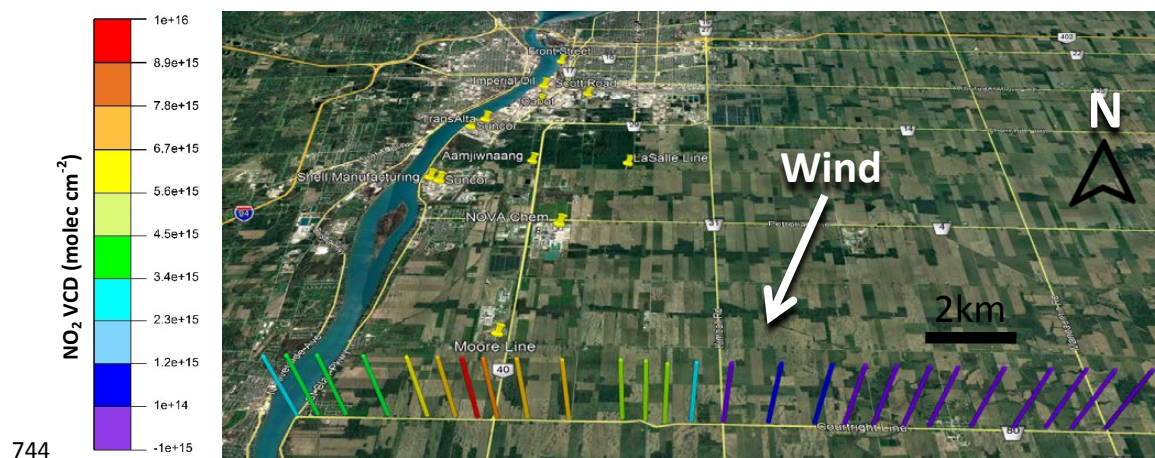
740

741

742

743

Figure 3 Day 1 driving routes; (a) route 1, (b) route 2 and (c) route 3, used to estimate NO<sub>x</sub> emissions from Sarnia.



744

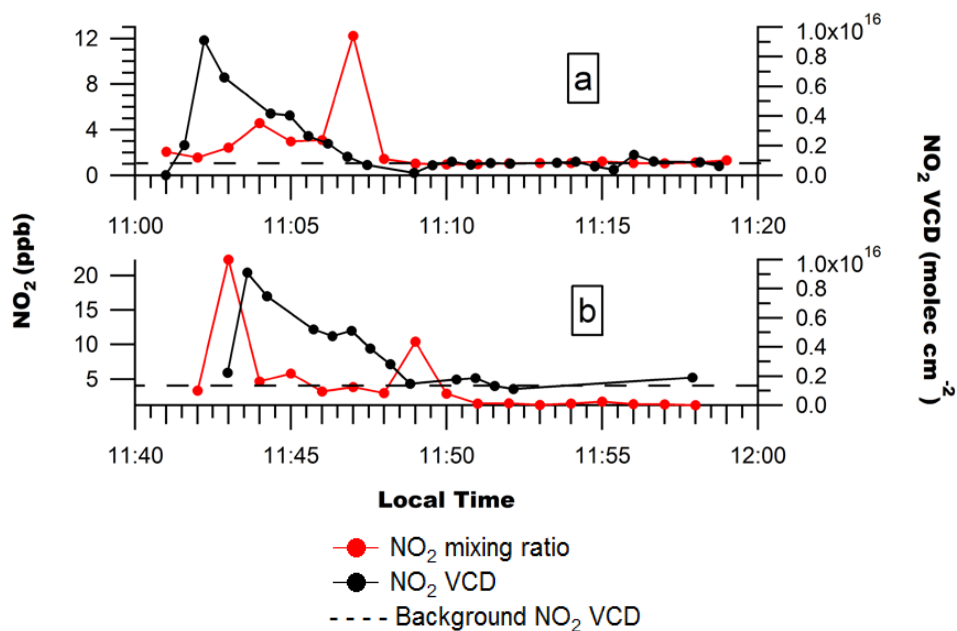
745

746 **Figure 4** NO<sub>2</sub> VCDs measured on Day 2 route 1.

747



748



749

750  
751

752 **Figure 5** NO<sub>2</sub> mixing ratios and NO<sub>2</sub> VCDs measured on Day 3 along (a) driving route 1 and (b) driving route 2.

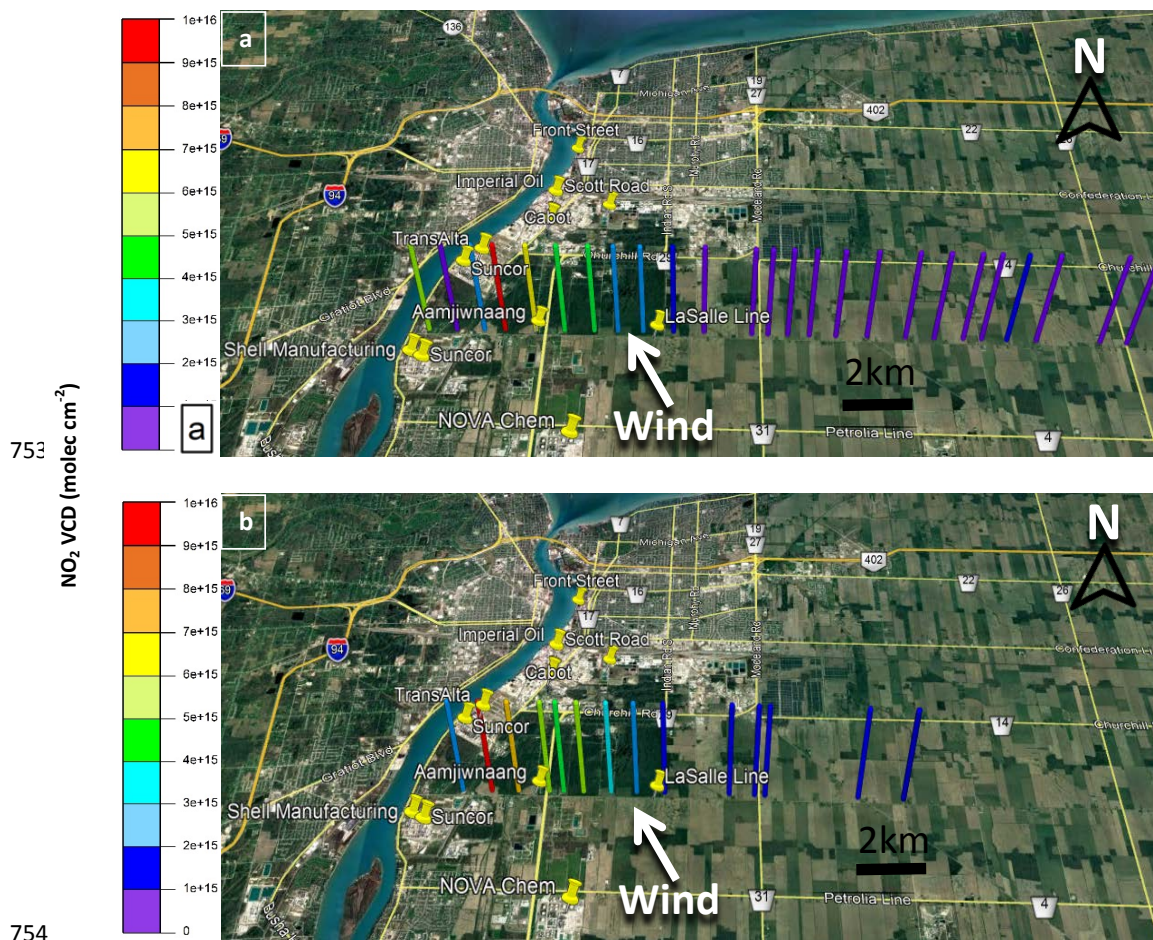
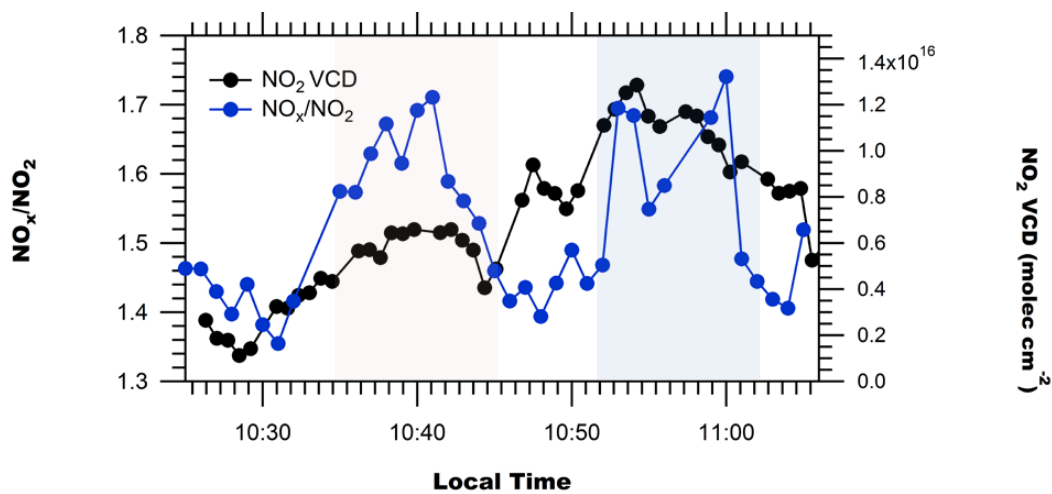


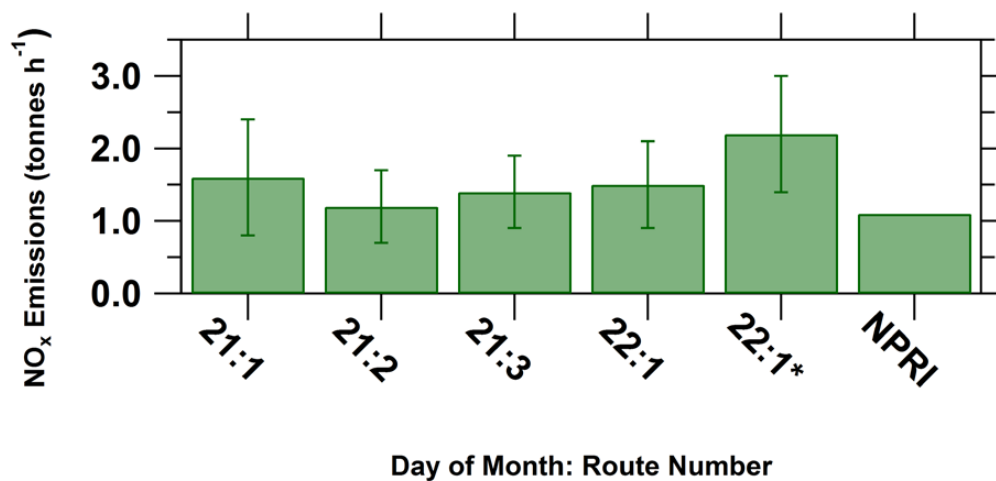
**Figure 6** NO<sub>2</sub> VCDs measured on Day 3 along (a) driving route 1 and (b) driving route 2.



757

758 **Figure 7** NO<sub>2</sub> VCDs and NO<sub>x</sub>/NO<sub>2</sub> ratios on Day 1 route 1. Detection of Michigan power plants' plume(s) (left) on  
759 East-West transect & Sarnia plume (right) on North-South transect are highlighted in pink and blue, respectively.

760



761

762 **Figure 8** Lower limit estimates of NO<sub>x</sub> Emissions from Sarnia on Day 1 and Day 3 and 2016 NPRI emissions. The  
763 22:1\* NO<sub>x</sub> emission estimate used individual NO<sub>x</sub>/NO<sub>2</sub> ratio values for each VCDs rather than a single average  
764 ratio.

765

766

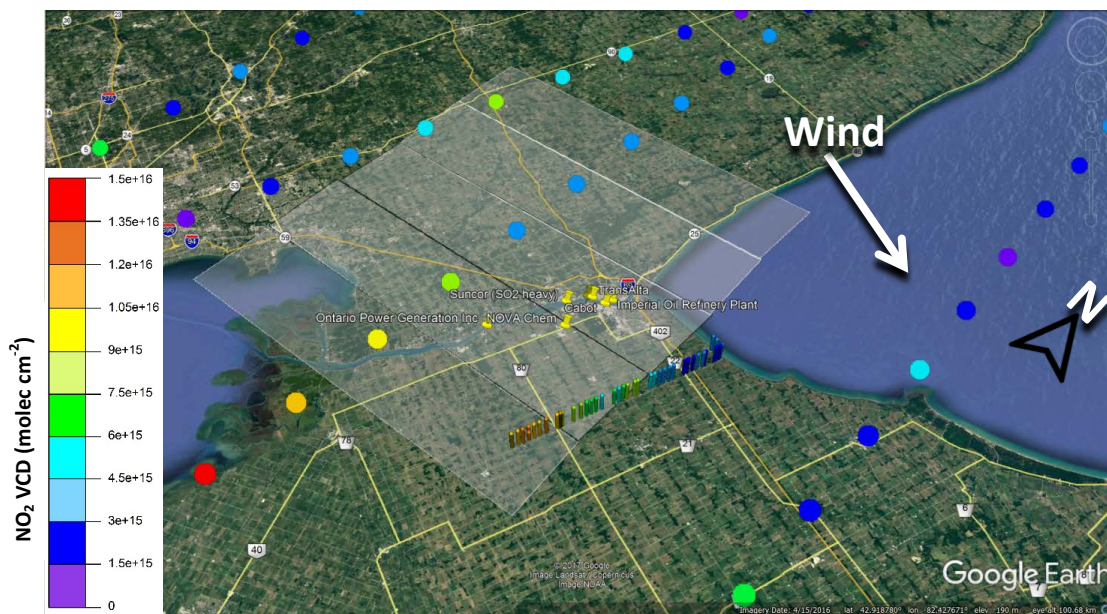
767



768

769 **Figure 9** SO<sub>2</sub> VCDs along route for emission estimate (Day 1 Route 3).

770

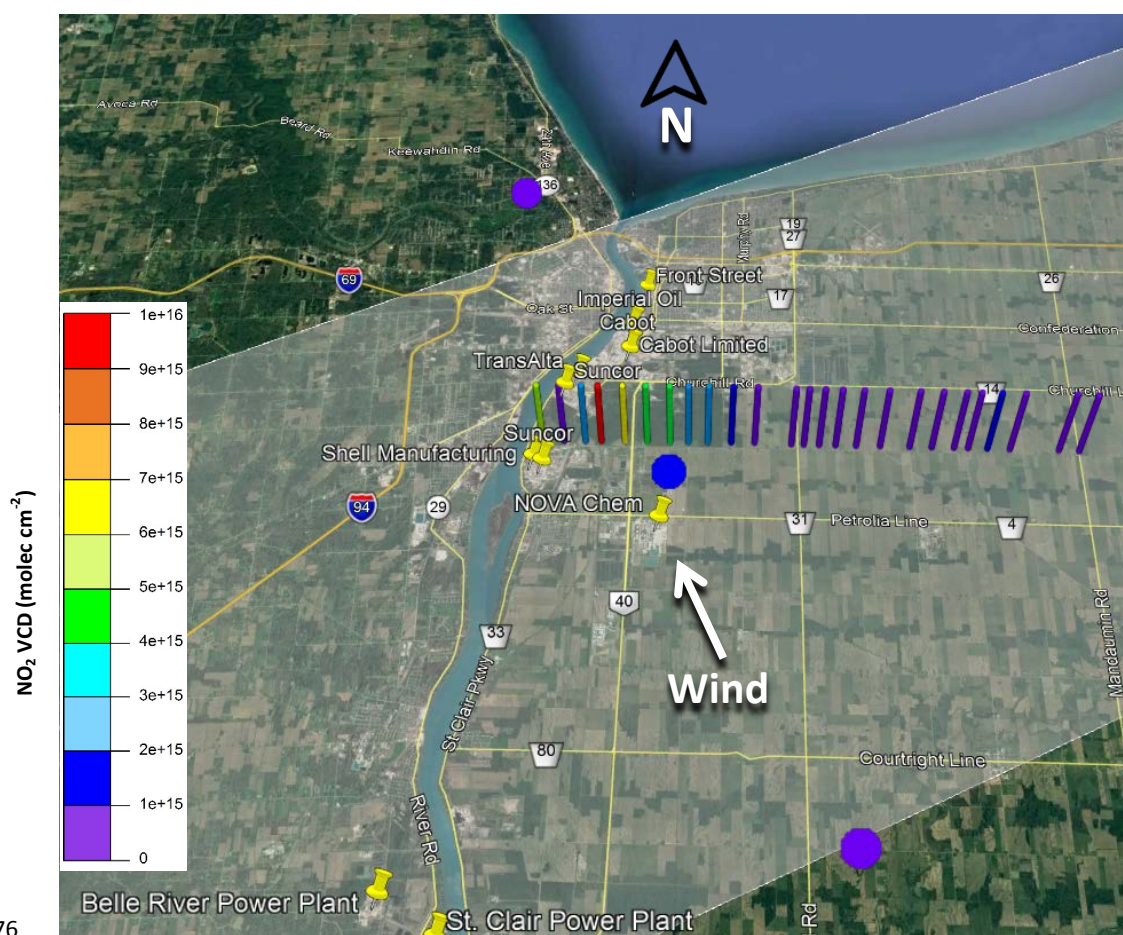


771

772 **Figure 10** Day 1 NO<sub>2</sub> VCDs from OMI satellite VCDs and mobile-MAX-DOAS Route 4. OMI satellite pixels  
773 closest to Sarnia were measured at ~18:00 local time. Semi-opaque rectangles centered on the colored dots  
774 (indicating satellite VCD value) indicate the spatial extent of the pixel.



775



776

777 **Figure 11** Day 3 NO<sub>2</sub> VCDs from OMI satellite and mobile-MAX-DOAS Route 1. OMI pixels shown were  
778 measured at ~18:00 local time. Semi-opaque rectangle centered on the colored dots indicates the spatial extent of the  
779 pixel.